SCALABLE AND CONTROLLABLE FABRICATION PROCESS FOR MEMBRANE MIRRORS

by

Phuoc Andy Phan

A Thesis Submitted to the Faculty of the

COLLEGE OF OPTICAL SCIENCES

In Partial Fulfillment of the Requirements

For the Degree of

MASTER OF SCIENCE

In the Graduate College

THE UNIVERSITY OF ARIZONA

2019

THE UNIVERSITY OF ARIZONA
GRADUATE COLLEGE

As members of the Master's Committee, we certify that we have read the thesis prepared by Phuoc Andy Phan, titled 'Scalable and Controllable Process for Membrane Mirrors' and recommend that it be accepted as fulfilling the thesis requirement for the Master's Degree.

Dr. Yuzuru Takashima Date: 5-7-2019

Dr. Dae Wook Kim Date: 5-7-2019

Dr. Chris Walker Date: 5-7-2019

Final approval and acceptance of this thesis is contingent upon the candidate's submission of the final copies of the thesis to the Graduate College.

I hereby certify that I have read this thesis prepared under my direction and recommend that it be accepted as fulfilling the Master's requirement.

Yuzuru Takashima Date: 5-7-2019
Professor
The College of Optical Sciences

ACKNOWLEDGEMENTS

I would like to share my great appreciation for everyone that has been a part of my journey during my time as a graduate student at the College of Optical Sciences. I would first like to express my deepest appreciation and thanks to Dr. Yuzuru Takashima, sensei, for the vast amount of guidance he has given me. I cannot express how much it meant to me and has helped me grow after being accepted into your group. It has allowed me to learn so much more about building and working on set-ups and approaching problems in different views than what I had known previously. You taught me that it is sometimes necessary to slow down my approach to getting better results, and how I should be presenting them to those that will be listening to my work. Above all, I appreciate your constant willingness to help in every aspect of my career and I hope to live up to your expectations.

I want to give my thanks to my family and friends. I would never be where I am without the support and push from my mom. With her telling me that she always wants what is best for me is what motivates me to this point. I give thanks to my dad who tells me to take things easy and not let everything consume me. To my brothers, my cousins, and my friends, the emotional support I get from you all has helped me when I have been at my lowest and has allowed me to continue to get to where I am now. I truly hope I will be able to make all of you proud.

Next, I would like to thank my two committee members Dr. Dae Wook Kim and Dr. Chris Walker who not only acted as my committee but were also my additional advisers. Dae Wook, your belief in always collaborating lead to me working in your lab. From there, I have met so many people that I thought I wouldn't have otherwise and that means so much for me. You welcomed me as a member of your lab, and I hope to be a student you can be proud of. Chris, so much credit goes

to you for me starting the work that I got involved in. I thank you for the support you gave in continuing any research that stemmed from your ideas. From working with you, I learned I can still think simple but still think big!

To my peers, colleagues, but also friends, I want to say thank you to Sunglin Wang, Logan Graves, Brian Kellermeyer, Brandon Hellman, Henry Quach, Dr. Heejoo Choi, Hyukmo Kang, and Isaac Trumper for all your input and advice you've given me on my research when I have been stuck. To Sunglin, thank you for giving me that push that I needed to do things I had to do ever since we were both in graduate school after undergrad. To Logan, thank you for the patience and support from our first project together; I learned so much about optics but also life balance from you. To Brian, thank you for enduring the troubles of building the mirror and the stresses it came along with it. To Brandon, Henry, Heejoo, Hyukmo, and Isaac, thank you for every ounce of help and advice you gave me regarding things even beyond my research. To the rest of the Takashima and LOFT Group, John, Yi-Ting, Marcos, Hyemin, Chuan, Trenton, Joel, and Ted, thank you so much for just your company. I learned so much more than I expected by talking with you all.

Finally, I want to give my appreciation to Dr. Koshel, Lindsay Loebig, and Mark Rodriquez. Thank you for all the support during my time here with telling me what I need to complete but also standing by my side when there were questions regarding my credits I had to meet.
Thank you to people that I did not mention here. Without your support, I wouldn't have gotten this far.

CONTENTS

LIST OF FIGURES

LIST OF TABLES

ABSTRACT

With the future need of larger telescopes, membrane mirrors are an option to create large-scale reflectors needed for space base observation at a lower cost than conventionally made mirrors. Proposed methods of how membrane mirrors have been put into place with ideas such as Dr. Chris Walker's inflatable spherical telescope and the L'Garde Inflatable Antenna Experiment (IAE). With data from L'Garde, Dr. Aden Meinel presented the curvature of a membrane mirror does not produce a spherical curvature. From there a look into what sort of aberrations that curvature produces and attempts to correcting it or processing it to other benefits by altering the material. Procedures will be done on a small-scale in a process that can be applied to larger-scale systems.

1 INTRODUCTION

For space-based telescopes, the desired trait is having a larger aperture. The larger the aperture a telescope has, first it allows more photons to be collected into the sensor so faint objects can be seen. Second, a larger aperture will improve the ability in resolving points when looking into space as a larger aperture would allow the minimum Airy disk diameter to reduce, consequently improving angular resolution. With larger reflectors allowing astronomers to gather more information of our universe. The planned launch of the James Webb Space Telescope has an effective aperture of 6.5 meters which is over 2.7 times larger than the Hubble. With the larger reflector, the James Webb Space Telescope will provide a larger range of studies over that of the Hubble.

Currently, the problems for these large-scale mirrors is fabricating and then transporting the telescope into space as the larger the mirror the heavier and more volume it is likely to take up. An alternative to traditionally made mirrors is membrane mirrors. The use of membrane mirrors would be a lightweight alternative that is scalable for different applications. Mylar is the name commonly associated with the reflective film. As Mylar was not created with the intended use of optical imaging, the stages of optical design, fabrication, and metrology are adjusted to fit this alternative material for telescopes. For longer wavelengths or lower frequencies, there are some prior designs to begin with. From there it is possible to see what fabrication process can be improved and controlled to maintain the quality needed as shorter operating wavelengths are reached. In following subsections, we address state-of-the-art, both in concept and actual implementations, of such membrane-based large telescopes as listed in Table 1.

Table 1. List of prior Mylar design and operating frequency/wavelength. Approximate weight of Mylar design and approximate weight of traiditonally made mirror.

Design	Size	Operating Freq.	Wavelength	Approximate weight	Approximate equivalent traditional weight
Small scale spherical receiver	1 meter (Sphere)	MHz-GHz	3000 – 30 mm	0.1kg	28 kg (CFRP, t=1cm, Hemisphere)
L'Garde Inflatable Antenna Experiment	14 meter (Double Sided)	GHz	30 mm	10 kg	2800 Kg (CFRP, t=1cm, 14m disc)
Terahertz space telescope	60 meter	THz	0.3 mm	390 kg	12000 kg (CFRP, Equivalent to 30m t=1cm disc)

1.1 Dr. Chris Walker spherical reflectors for space-based telescopes

A proposed concept of using Mylar as a space-based telescope is an inflatable spherical mirror by Dr. Chris Walker from the Astronomy Department at the University of Arizona. With this proposed design it is possible to inflate a large spherical balloon and aluminize a subsection to use as a primary reflector.

1.1.1 Small scale flight unit

Dr. Walker adapted his idea to a small-scale test flight unit for telecom use but would operate as far as 8 GHz, 3.75 cm wavelength which is in the microwave spectrum [2]. Observing Fig. 1, the Mylar pieces are stitched together to create the spherical shape. As this is operating frequency is in

the MHz and into the early GHz, the stitching of the Mylar is likely not to cause any issues with collecting the energy it is oriented at.

Figure 1. Image of stratosphere test flight with a 1-meter sphere for telecom. Image courtesy of C. Walker; funded by the Office of Naval Research and Free Fall Aerospace.

1.2 L'Garde Inflatable Antenna Experiment

Another design that had incorporated the use of Mylar as the primary reflector was the L'Garde Inflatable Antenna Experiment (IAE) to create a low cost and lightweight space antenna [4]. L'Garde, Inc was a task in developing this structure for the possible use of mobile communications, earth-observation radiometry, microwave sensing, and Department of Defense space-based radar.

This experiment consisted of a 14-meter parabolic reflector which was developed based on a 9-meter parabolic test design. The IAE was carried and deployed by the Spartan 207 on the STS 77. When deploying the antenna, the structure successfully arranged itself to demonstrate the robustness of the structure. The only concern from this was the deployment happened in an uncontrollable manner. What caused this uncontrollable deployment was due to residual air in the stowed structure

for the membrane primary. As a result of the residual air, the struts that held the primary to the instrument cluster extended in series rather than concurrently as planned. Inflation gas for the IAE was also not introduced as the inflation system malfunctioned. As a result of the malfunction, the membrane reflector did not fully expand to the intended to achieve operation. The uncertainty and malfunction aside, the experiment was able to validate its potential for a new space structure for low-cost missions.

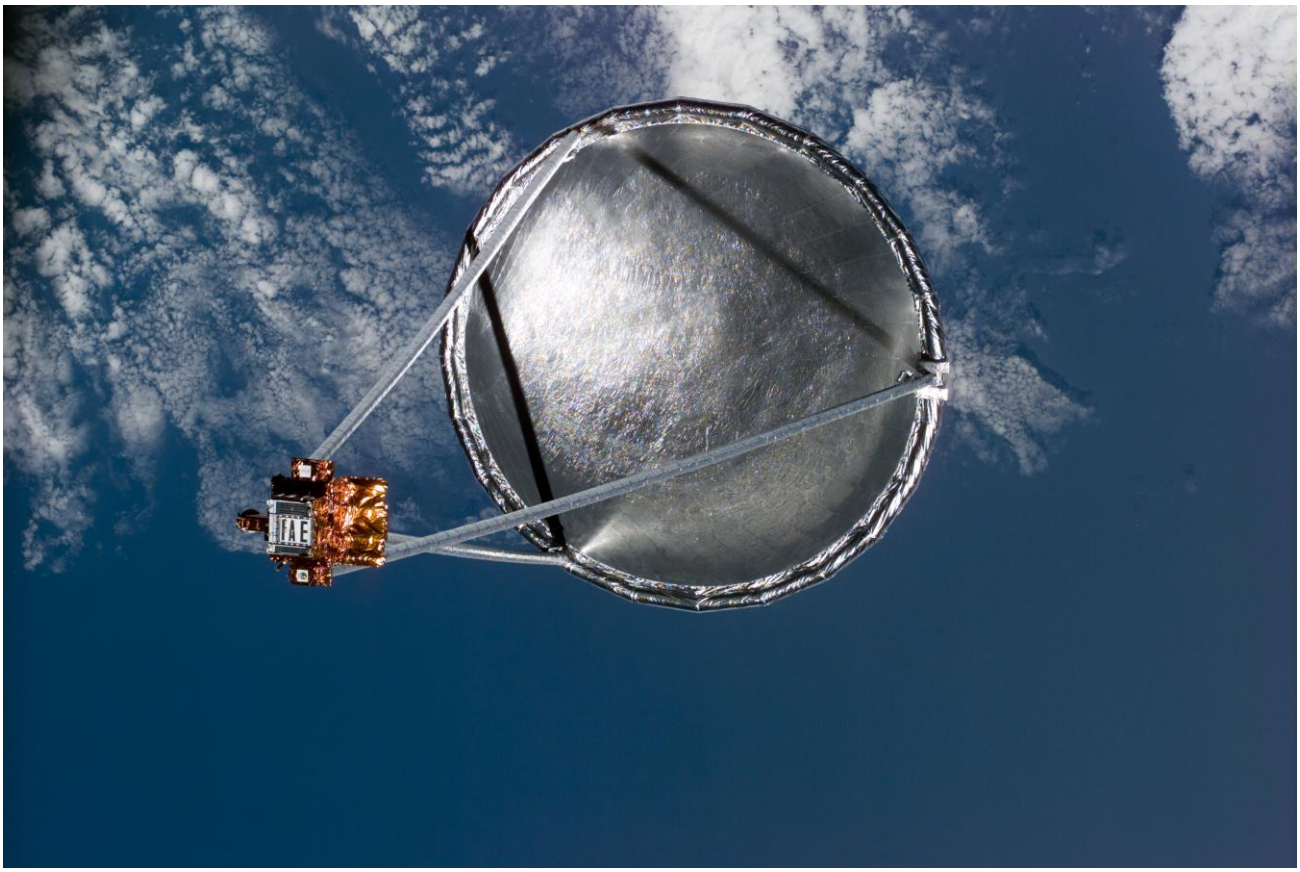

Figure 2. Image of L'Garde Inflatable Experimental Antenna

1.2.1 Terahertz Space Telescope

Dr. Walker's overall concept is to have a large inflatable structure to form a 60-meter sphere with a 25-meter spherical mirror segment [1]. With this design as an option for larger and affordable

aperture for the far infrared range. This solution provides an option for mirrors on a much larger scale than has been launched which would lead to being able to resolve much higher details. Subsystems would include a spherical aberration corrector, a deflectometry system to monitor the shape of the mirror on orbit, and potentially with an adaptive optics: a deformable compensating mirror. These subsystems are to address the limitations of the design of the primary mirror.

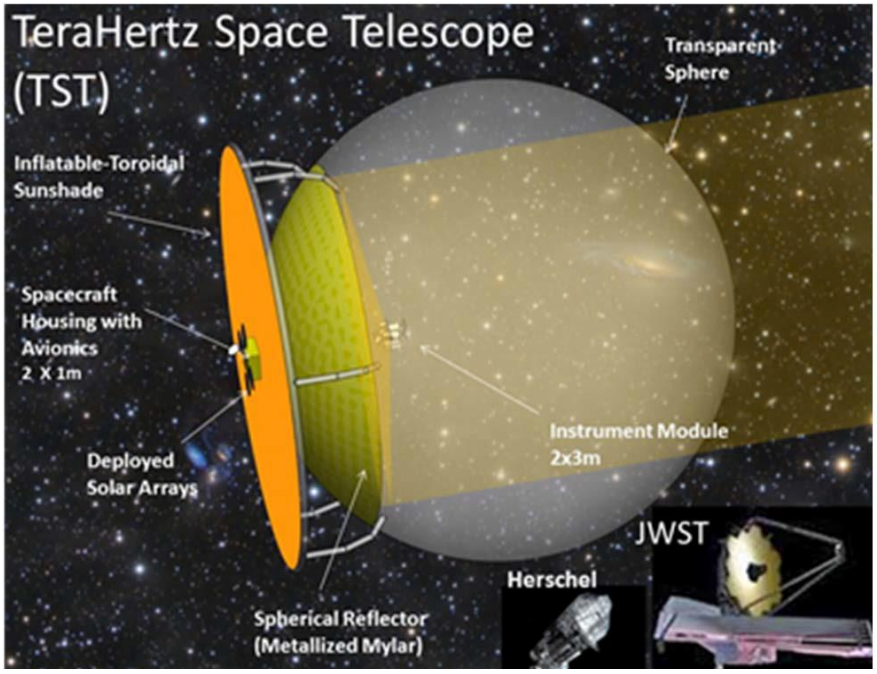

Figure 3. Image of the concept of the inflatable spherical telescope of the size a ~60-meter diameter sphere with a 25-meter section utilized as a spherical corrector shown alongside scale comparison of JWST and Herschel.

1.3 Mylar mirror for shorter wavelengths

When operating at MHz to GHz to THz, the expectation for the optical surface must improve to meet the corresponding standards, such as λ/4 waves in peak-to-valley of the surface figure. Reasons for this is when moving to a higher frequency the amount of scattering is more noticeable due to imperfections of the surface. Also, the surface figure must be precise enough to suppress wavefront aberration. Since a λ/4 waves peak-to-valley standard of precision is wavelength dependent, as the

intended wavelength gets shorter the precision of the surface will get tighter. Scattering by the roughness of the mirror surface is another factor to be addressed. The surface roughness of Mylar is spec'd at 38 nm [3], which should be reasonable for use in the THz range. With that in consideration, a look into the fabrication process that is needed to best construct precisely shaped, lightweight and controllable inflatable mirror from Mylar will be performed as to maintain the accuracy of the surface, though we expect that it is nor sphere nor a well-known conic surface, along with optical design to correct for aberrations specifically induced by such mirrors.

Research was done by Dr. Aden Meinel for the theoretical shape of an inflatable thin membrane mirror by formulating deformation of thin membrane mirror [5]. The theoretical model was refined by looking over the data from the L'Garde IAE which provided a better understanding of membrane mirrors. Also, another type of primary mirror, spherical mirror, aberration correction optics has been researched and implemented to a system, such as the Hobby Eberly Telescope, as described in later section [5,6].

This thesis addresses the fabrication aspects of Mylar mirrors. In the past, a similar attempt was made for using a Mylar mirror in the visible wavelength. When considering making a testing mirror, the priors space telescope designs have a fabrication trait in common, inflation by differential pressure. As these designs mainly focus on a subsection of a larger base curvature, the experimental mirror will be made to focus on just this. Prior work was conducted with pneumatically-formed metalize polyester mirrors was written by Bruce Holenstein. In the paper, the motivation and result are detailed, but no fabrication details and only images of the mirror are provided [8]. With the images, a small-scale mirror our own can be made to begin experiments and fabrication process can be laid out. A secondary design to test is like the IAE of L'Garde and a patent on air heating

polyethylene balloon by Ehrreich, John E., Charles P. Fazio, and Beverly A. Nickerson [9]. Last, a look into fabricated vacuum molded mirror will be tested to compare to the differential pressure membrane mirrors as a viable option for use alternative membrane systems.

This research will explore an annealing method, a heating technique, so Mylar will be allowed to smoothly stretch which will allow the mirror to inflate to the desired curvature with less effort. Having that would lead to requiring less inflation gas which could possibly solve the issue that L'Garde had during their IAE test.

Chapter 2 addresses the theory on the deformation of thin flat, uniform, isotropic and circular membrane under pressure. Chapter 3 describes experimental work to quantitatively identify the radius of curvature of such a deformed mirror under pressure. Also, the effect of pre-annealing and In-situ annealing are addressed. Double sided mirror concept is also demonstrated on a small scale. In chapter 4, explores the use of polyethylene terephthalate, commonly abbreviated PET, as mirrors by vacuum molding the material to a template surface.

2 THEORY

2.1 Dr. Meinel and Hencky surface

Dr. Aden Meinel revisited the use of membrane mirrors for visible imaging by re-analyzing data provided by L'Garde for a 900 mm diameter Mylar mirror. Such inflated mirrors have been used for cases that low acuity in imaging is adequate; for example, microwave antennae and solar energy concentrators. Dr. Meinel states that these membranes mirrors are neither spherical or parabolic but can be expressed by an even power series known as the Hencky curve. The equation for the Hencky surface can be expressed as:

$$z(u) = \frac{D}{64F^2}(u^2 + 0.1111u^4) \tag{1}$$

Central deflection of a circular thin plate, like a thin membrane, corresponds to the sum of the bending mode and stretching mode which can be interpreted as the inverse central deflection. For a thin plate, the bending is the dominant part of the summation, but when considering a thin membrane, it is the stretching that becomes dominant.

$$\frac{1}{z} = \frac{Et^3}{k_1 \mathrm{P}\, \mathrm{r}^3} + \frac{E^{\frac{1}{3}} t^{\frac{1}{3}}}{k_2 P^{\frac{1}{3}} r^{\frac{4}{3}}} \tag{2}$$

Bending Stretching

The theory behind the shape of a thin plate with a specific diameter and uniform pressure for a normalize term u is given by:

$$z = \frac{kP^{\frac{1}{3}} D^{\frac{4}{3}}}{E^{\frac{1}{3}} t^{\frac{1}{3}}} f(u) \tag{3}$$

t is the thickness of the plate, E the modulus of elasticity and u= 2x/D, the fractional radial distance from the center of the membrane. For an inflated membrane of uniform thickness k = 0.248. Equation f(u) is the general equation for a Hencky surface using terms up to u^4. Using a = 0.9 for a classical Hencky that would yield the following equation.

$$z = \frac{0.248\, P^{\frac{1}{3}} D^{\frac{4}{3}}}{E^{\frac{1}{3}} t^{\frac{1}{3}}} [0.9u^2 + 0.1u^4] \tag{4}$$

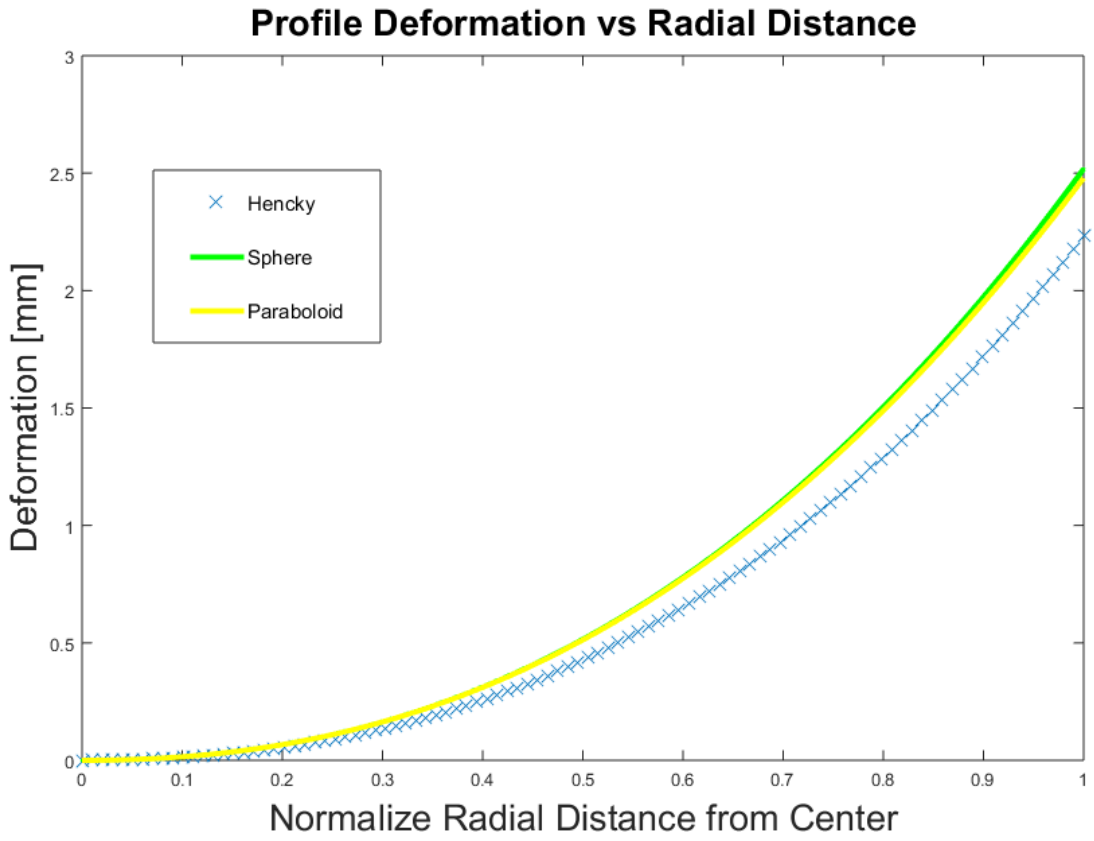

Figure 4. Profile comparison of a spherical curve, parabolic curve, and Hencky curve. The figure shows when compared to common surfaces used in optical design, the Hencky curve extends more into the radial direction quicker.

When re-analyzing the data from L'Garde, Dr. Meinel plotted the data and then subtracted a best fit parabolic curve. In doing this he noticed a tilt in the resulting curve that is generally associated with coma. To examine a possible asymmetry, the data from L'Garde was compared between two orthogonal azimuths on the mirror. This was done by repeating the plot of the curve data and then removing the parabolic curve for both orthogonal directions. The results were the curves were similar in curvature but had a difference in height. This difference leads Dr. Meinel to say the data from the mirror by L'Garde was astigmatic.

3 EXPERIMENT

3.1 Test set-up

The basic experiment set up for each type of membrane mirror is a point to point imaging system. First, a He-Ne laser (Thorlabs Model # CPS180) is focused on using a microscope objective lens. When the focal point is placed at twice the focal length in front of the mirror it is the position of the radius of curvature R, equivalently the paraxial focus is R/2, the spot produced at the focal point with a magnification of 1 magnification. At this distance is also the radius of curvature. From there the mirror measured radii can be compared to its designed radii or what alterations have been made. The radii were identified by finding the minimum spot location by moving point source back and forth while keeping the distance from the mirror to the camera (Thorlabs Model # DCC1545) the same as the distance from the mirror to point source.

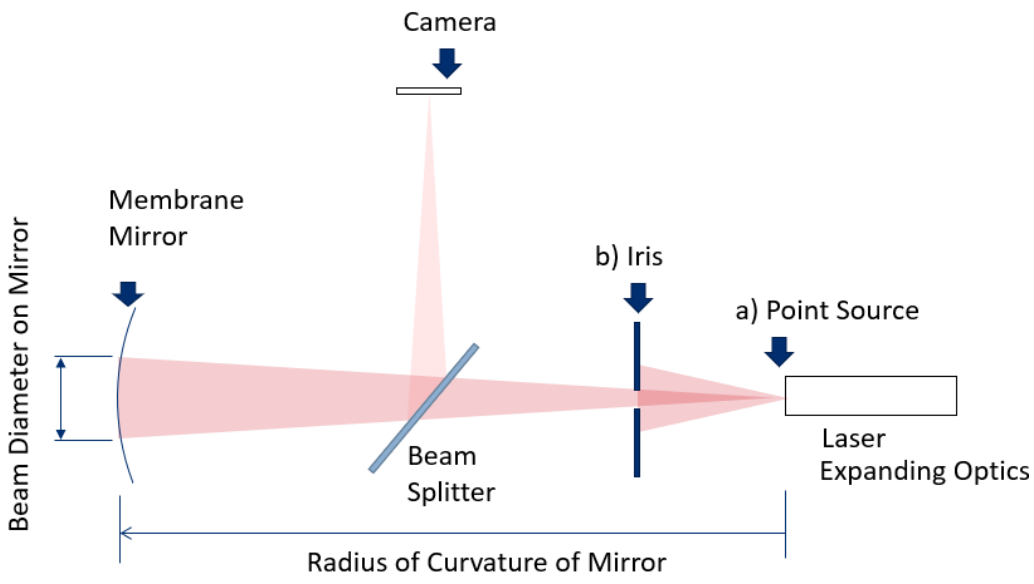

Figure 5. a) Point source placed at the radius of curvature (ROC) of the mirror. b) The iris in the setup is used to control the beam diameter on the mirror.

3.2 Mylar mirror fabrication

The Mylar mirror fabrication and test system are schematically depicted in Fig. 6. The system consists of two 50 mm inner diameter vacuum flanges (Duniway F0338-200R) attached to a cylindrical chamber in which the negative pressure is applied. The attached chamber is composed of 50 mm diameter by 100 mm length PVC pipe. Attached to the opposite end is a 3D printed endcap for the pump that will be applying the negative pressure. The connection points between the flange, PVC pipe, 3D part, and pump line are held together with silicone sealant. This ensures there are no air leaks from the hardware. The only possible air leaks would only be from the Mylar itself. The Mylar itself is held in between two copper gaskets, which is then held between the two flanges that are tightened to create the closest possible vacuum seal. Negative pressure is created by (ZENY Model VP 125+) while being monitored and regular by (Marsh Bellofram, Model # 35102709). Figure 6 shows the set-up of the Mylar mirror set-up. Figure 7 shows the vacuum process of monitoring.

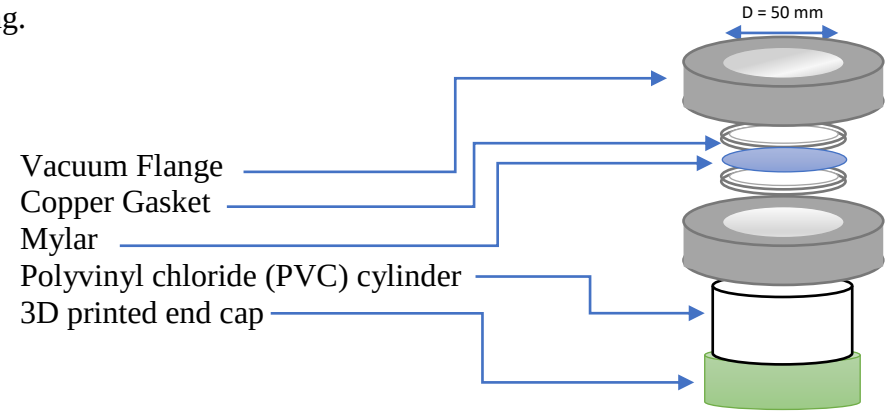

Figure 6. Contacts between end cap, cylinder, and bottom flange sealed with silicon. Flanges held together with eight screws.

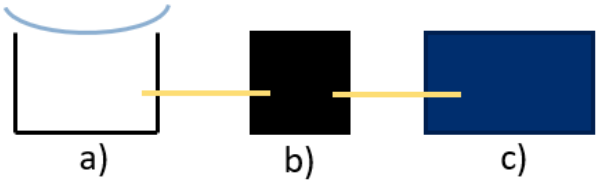

Figure 7. Vacuum path starting with a) Mylar mirror chamber having negative pressure applied by c) vacuum pump that flows through b) air regular to maintain selected pressure on Mylar.

3.2.1 Initial set-up with 3 C-clamps to set up with 8 screws

Initially, the system was tightened together using 3 C-clamps. This caused problems as it made the mirror repeatability unreliable due to the pressure from each clamp. The switch to using eight screw holes that were present on the flanges was preferred but perforating the Mylar to allow the screws to go through without damaging the main viewing Mylar was the following problem. The decision was made to trim the Mylar to the shape of the copper gasket. This solved the problem of damaging the Mylar while allowing the screw bolts through and providing a more consistent method of tightening the flanges together. The bolts were tightened using a cross pattern, which is tightening one screw then moving to the opposite side to insert the following screw repeating these two steps until all fittings are filled. This method allows for more consistent pressure applied and reduced flex on the copper gaskets.

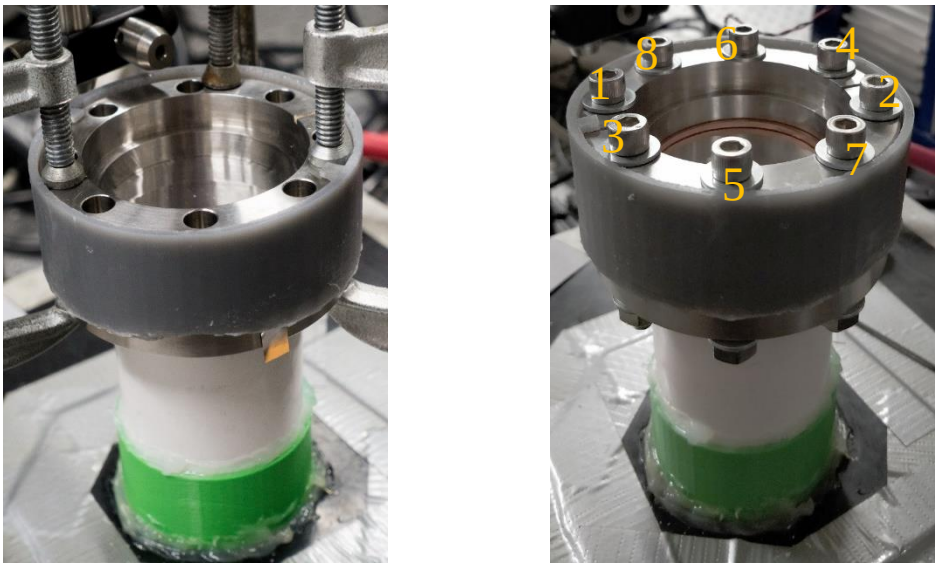

Figure 8. Mirror set up with three clamps holding flanges (left). Mirror set up with eight screws holding flanges (right). Numbers displaying order of tightening screws.

3.2.2 Sealing process by using IPA

For the first trial, the system pressure stability was at 0.2% of the vacuum regulator. On testing the repeatability of the system for a future test, the vacuum stability started becoming inconsistent having pressure stability of 5%. Some procedures were put into place for more consistent repeatability in the system build. The main change that helped the vacuum stability was applying IPA on to the copper gaskets before setting the Mylar between the two gaskets. This procedure assures close contact between the Mylar membrane and gaskets by employing capillary force and evaporation of IPA. Possibly also having a clean surface allows the Mylar to create a better air seal. This procedure is also extended to the flange faces. After this change in procedure, the stability of the vacuum regulator was reduced from 5% to 0.3%; a more manageable working range.

To add to the procedure of setting the Mylar into the system to produce a stable mirror, the tightening of the screws was also given an order of operation. Each step done in the previously

mentioned cross pattern, the eight screws are first tightened by hand until tension from flange face can be felt. Once the eight screws have been tightened by hand, the screws are then tightened with a screwdriver while the bottom nut is held by a wrench; again, the screwdriver is tightened until there is tension with slight effort. Finally, the bottom nut is tightened with the wrench until tension stops the wrench.

3.3 Mylar mirror radii vs pressure

Using the mirror in the point to point imaging set up, it was possible to measure a rough order of the value of the radius of curvature by adjusting the position of the point source until the returning spot size matches the iris size. The values were taken from -2% (-0.3 psi) of the total pressure to -15% (-2.25 psi) of the total pressure. Max pressure of the pump being used was -15 psi, so the range of pressure used was -0.3 psi to -2.25 psi. Each percent equals -0.15 psi change in pressure. Figure 9 shows the progression of the radius of curvature with respect to the increased negative pressure applied. It was observed that the change in radius of curvature to pressure was quadratic. Using the radius of curvature measured from the experimental set-up, the associated sag for each radius of curvature can be determined. With the sag values at each pressure, a comparison can be made to the theoretical Hecky deformation seen in Fig. 10.

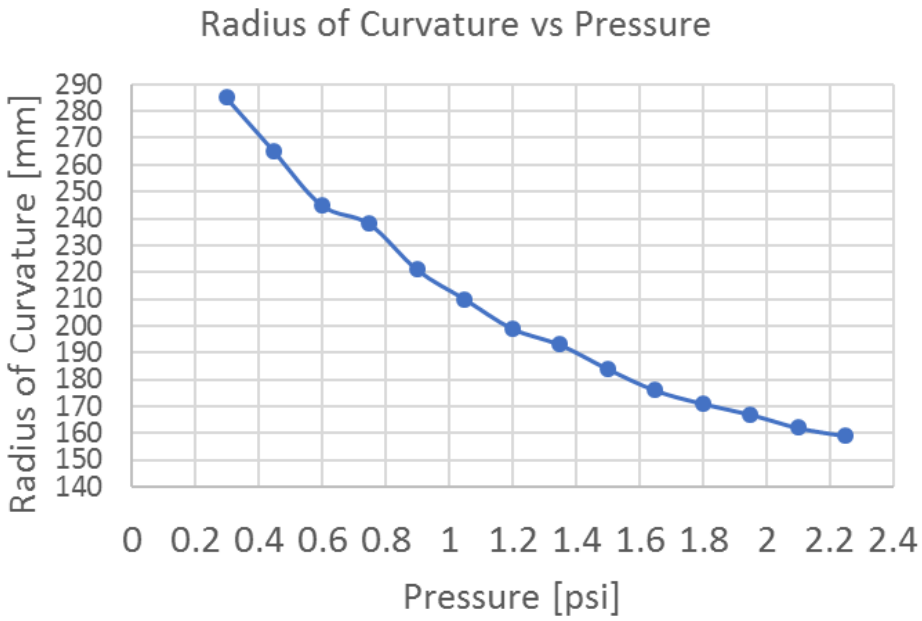

Figure 9. Plot showing change of radius of curvature vs increasing negative pressure applied. The relationship of the radius of curvature to pressure is quadratic.

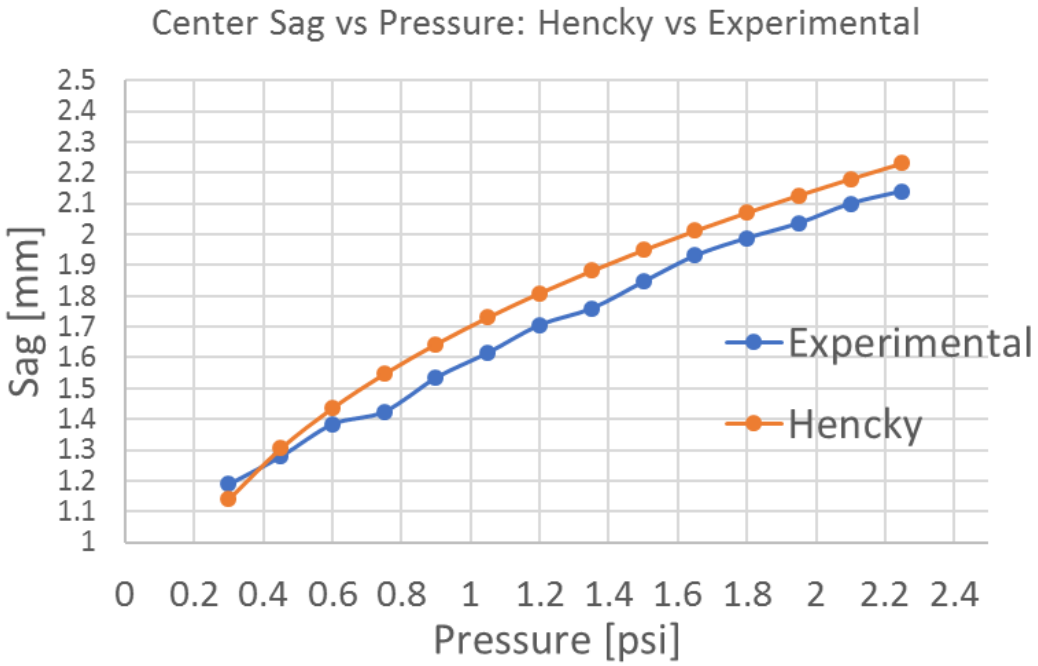

Figure 10. Theoretical Hencky deformation vs Experimental sag.

3.4 Material anisotropy

Through the first inspection of the spot produced from the Mylar mirror, there was clearly astigmatism. Figure 11 shows the variation of the spot shape as a function of detector position. The data was taken for -2.25 psi and the position of the point source is 100 mm from the mirror. Then detector was defocused for +7.5 mm from the medial focus that corresponds to Sagittal image, and -7.5 mm from the medial focus for Tangential image. The test was repeated for a laser beam size of 10mm and 40mm on the Mylar mirror. It was discovered that the way Mylar is produced by heating polyethylene terephthalate and stretching it out into a film [10]. This process likely causes the Mylar to stretch a different amount orthogonally to each other. Figure 12 shows testing of the astigmatism present is caused by the stretch in the processing of the Mylar, the film was set in one orientation and had the spot image captured. Next, the film was rotated 90 degrees and the resulting spot was observed to have also rotated 90 degrees from the previous orientation. From this, it is possible to conclude that the astigmatism present is mostly due to the method by which the Mylar is processed.

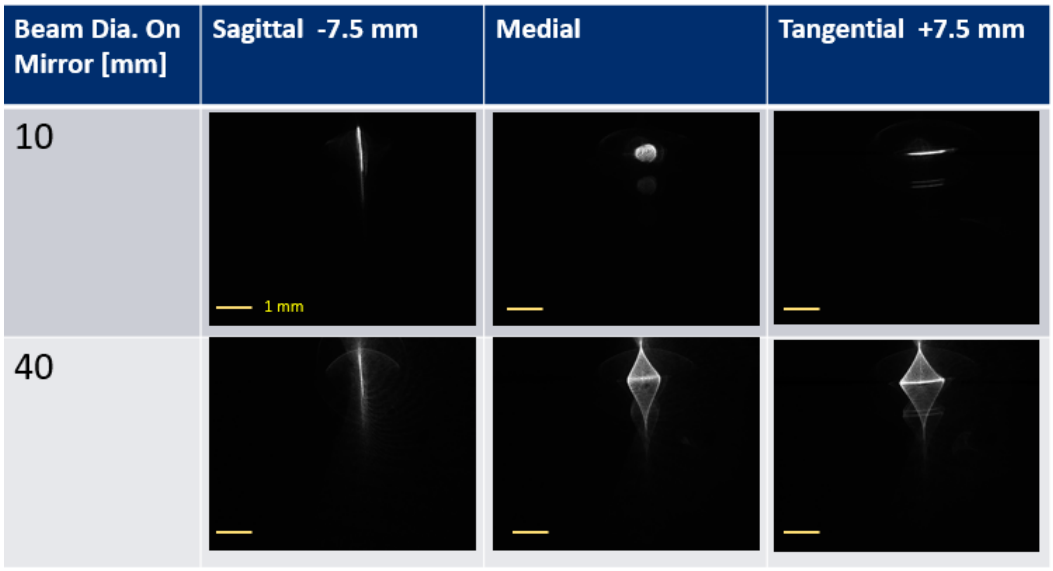

Figure 11. Image sequence of through-focus from sagittal to medial to tangential focus at -15% pressure (-2.25 psi) with an equivalent radius of curvature of 160 mm. Defocus between sagittal and tangential focus 10 mm.

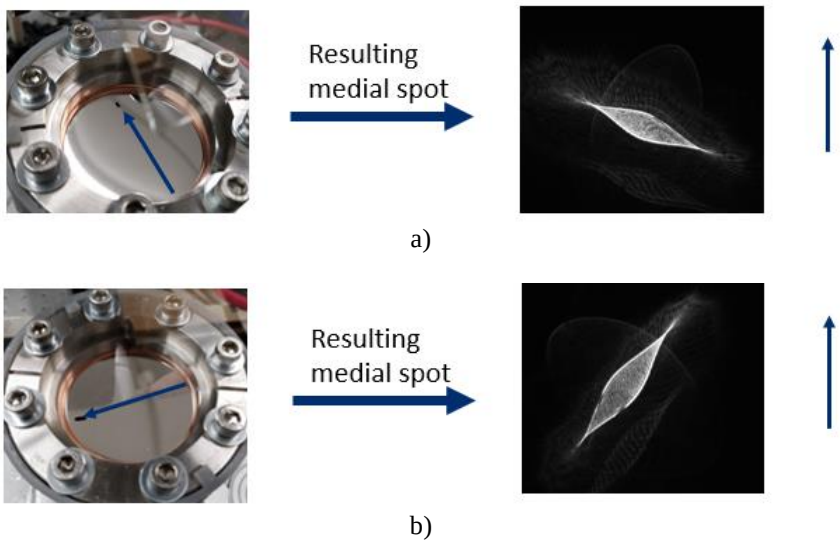

Figure 12. Image a) first orientation of Mylar with resulting medial focus followed by rotating Mylar in image b) resulting in the medial focus spot also rotating 90 degrees.

3.5 Astigmatic shape relation to aperture

In the test set up the incoming beam would be stopped down with an iris. When this was done, the spot produced wouldn't reduce in size with the same astigmatic shape. It is known the spot produced by the Mylar mirror is a combination of astigmatism and spherical aberration. What is likely happening is when a larger diameter beam is incident on the mirror it allows for higher orders of spherical aberration to contribute. When the beam is stopped down to a smaller diameter, the contribution of spherical aberration is reduced, and the spot begins to scale with respect to astigmatism ray equations. Referring to chapter 2, equation 1 Dr. Meinel expressed as the Hencky curve is dependent on the external pressure the membrane is experiencing and the diameter the membrane is mounted to. Through this observation, the astigmatic shape of the spot looks to have the same relationship to the mounting diameter like the Hencky equation.

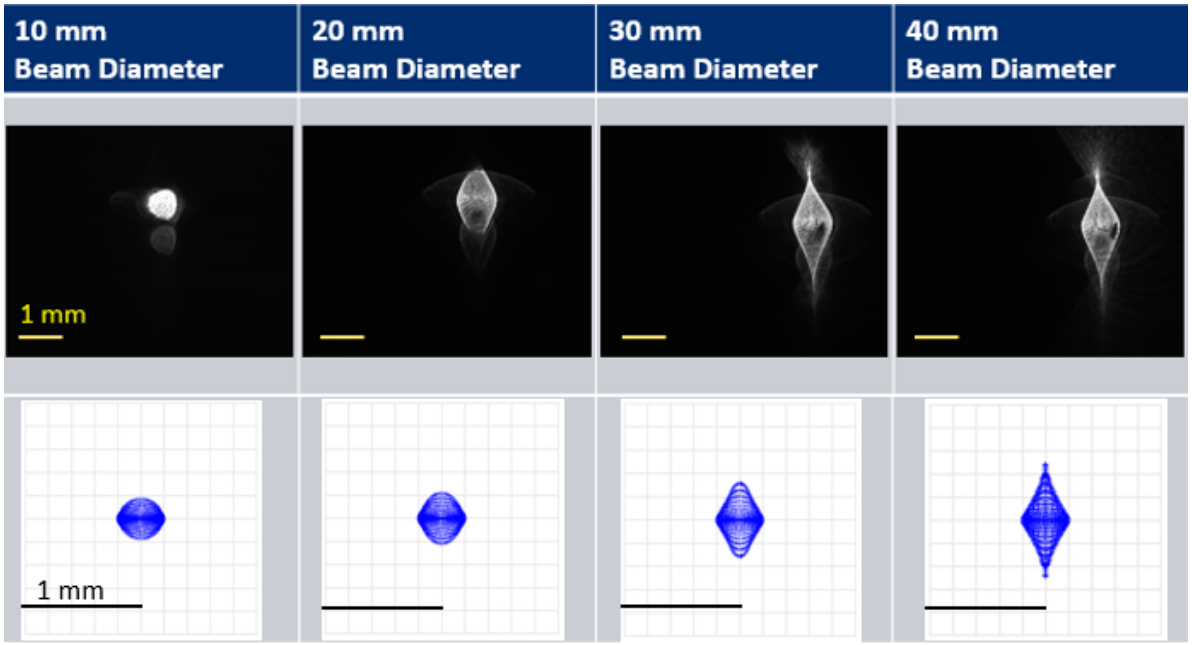

Figure 13. Change in spot size and shape as beam diameter increases. Comparison of spot diagram from lens design simulation.

3.5.1 Astigmatism and spherical aberration

It was noticed when the beam size on the mirror was reduced from 40 mm to 10 mm the resulting spot it produced would be what is expected of third order astigmatism in an optic; a sagittal, medial, and tangential focus. When the beam diameter of the point source was increased, with the camera set at the medial focus, the resulting spot would not be a circular spot that is expected of the medial focus. The resulting spot would best be described as a vertical focus almost coming into focus. The point that one would assume closely resembles a medial focus happened to be where the mirror produced a horizontal line focus.

To better understand why this mirror was producing this sort of spot, the mirror was modeled in Zemax OpticStudio. The mirror was set as an anamorphic surface with a parabolic conic. The base radius of curvature was set to -250 mm as this value was a radius of curvature that was observed in the initial observation. With the mirror surface defined as an anamorphic the x and y-

axis can be set with slight differences in radius of curvature; in this simulation, the difference was 0.008. This is done as we know the Mylar mirror as made is not spherical but has astigmatism present. With this, it was possible to simulate a similar through focus spot diagram as was being viewed from the built Mylar mirror.

	Surface Type		Comment	Radius	Thickness	Material	Coating	Semi-Diameter	Chip Zone	Mech Semi-Dia
0	OBJECT	Standard		Infinity	250.000			0.000	0.000	0.000
1	STOP	User Defined	US_ANAMR.dll	-250.000	-252.525 M	MIR...		24.877	-	-
2	IMAGE	Standard		Infinity	-			0.245	0.000	0.245

Conic	TCE x 1E-6	Cx	Cy	Kx	Ky
0.000	0.000				
-1.000	0.000	-4.000E-03	-3.980E-03	-1.000	-1.000
0.000	0.000				

Figure 14. Zemax prescription for Mylar mirror spot simulation.

Figure 15. Through focus of spot diagram from Zemax simulation of non-axially symmetry of the Mylar mirror.

When decreasing the entrance pupil diameter of this mirror, the contributing rays from the outer portion of the mirror causes the spot diagram to reduce until it is a circular shape at medial focus. By decreasing the entrance pupil diameter, the amount of spherical aberration due to the Hencky curve is reduced until the majority aberration is astigmatism seen in Fig. 13.

3.6 Elliptical gasket

Through the experiment and ray trace analysis, the astigmatic spot is attributed to how the Mylar film is fabricated. To correct for the intrinsic astigmatism, one possible way is to control how the boundary of the film is constrained while applying negative pressure. A possible solution is to mount the Mylar using elliptical gaskets over circular gaskets. The theory behind this is simply that the amount of curvature is different between the orthogonal axis. Then possibly restricting the aperture in which the Mylar can anchor the curvature from could provide a correction.

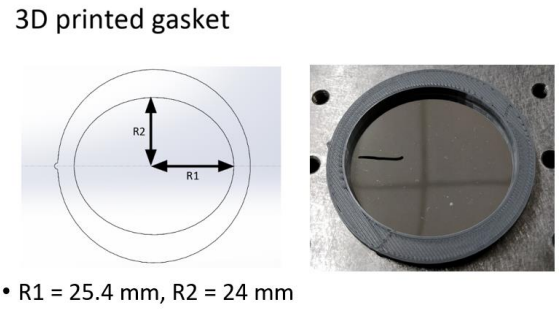

Figure 16. 3D printed elliptical gasket for controlling astigmatism seen in Mylar mirror.

For an inexpensive and relatively quick process, the gaskets were 3D printed. Without knowing how much an elliptical gasket would affect the spot or astigmatism, the first gasket was made to have r1 = 25.4 mm and r2 = 24 mm. The printed gaskets also had a notch added in the design to know which axis the long radii were. Figure 17 shows the spot for R = 193 mm at -1.35 psi with a beam diameter of 30 mm. The image was taken at medial focus point approximately 100 mm from the mirror.

Figure 17. Comparison of circular copper gasket (left) versus Mylar aligned to the short and long axis of the elliptical gasket.

Looking at the results, the elliptical gasket made the astigmatic spot larger. What is positive about this is that when the gasket is rotated, without the Mylar being rotated, the orientation of the spot also rotates. This proves that it could be possible to correct astigmatism in the Mylar with these elliptical gaskets.

3.7 Double layered orthogonal orientation

Since the Mylar has some directionality manufactured into it which induces some astigmatism when mounted with negative pressure applied to it. The idea came up to layer two Mylar films on top of one another and orient the directionality orthogonal to each other. The Idea behind this is to let the axis that is stretching more be braced by the axis that is not stretching as much. Unfortunately, this did not reduce astigmatism seen in the spot. Rather it made the seen astigmatism worse as the spot size increased. For the lowest pressure used, the entire spot could not be fully captured on the camera sensor.

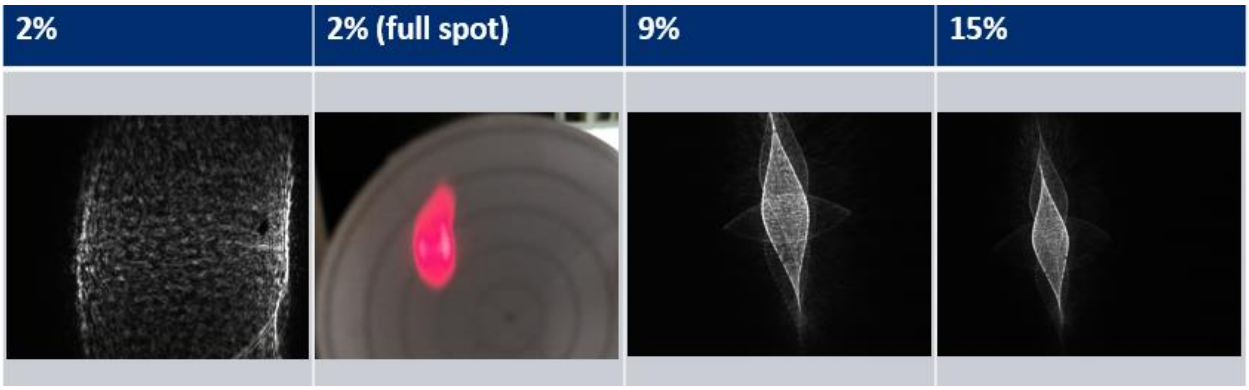

Figure 18.Image results from double Mylar layer experiment.

3.8 Mylar annealing

Method of fabrication can aid in the operation of a Mylar mirror. Referring to section 1.2 on the L'Garde IAE, it was mentioned that the antenna failed because the main chamber of the mirror was not able to fill to the desired pressure intended to operate. This is where annealing the Mylar can assist in that by stretching the film, therefore less pressure would be needed to obtain a specific radius of curvature. Three forms of annealing will be explored, pre-mount annealing, in situ annealing, immersion annealing. The first method will experiment on applying heat to the Mylar to induce more stretching when it is mounted into the system. The second method will have the Mylar mounted into the system and heat applied while the mirror is operating with the negative pressure. The third will incorporate an alternative design and combine aspect of the two previous annealing techniques by employing better heat transfer while the Mylar is mounted.

3.8.1 Mylar pre-mount annealing

3.8.1.1 Set-up

In discovering that how the Mylar is manufactured is the reason for the seen astigmatism in the spot image, the method was thought of to try and correct it. A technique known as annealing is used on materials to alter its physical and at times its chemical properties. The set up for our pre-

annealing involved the Mylar being set between two ground glass pieces. This is then set on top of a hot plate to induce the temperature that we desire for the annealing.

3.8.1.2 Testing temp

Figuring out the temperature to begin testing at initially was based on the Mylar value thermal coefficient of linear expansion, 1.7×10^{-5} in/in/°C [3], expressed as a ratio of change length over initial length multiplied by the change in temperature. Since the value of the thermal coefficient was low, it was thought that starting at a higher temperature would yield a more significant result to observe if it was needed to go higher or lower in temperature. The starting temperature for the first test was at 140° C for one hour.

After observing the image of the spot after the Mylar had been annealed at 140° C, it was determined that it was best to do further experiments at a lower temp as Mylar seemed to have more wrinkles introduced from being heated at 140° C. Using a new piece of Mylar for each test, the pre-annealing was done at 120° C and 100° C for one hour each. Figure 19 shows the pre-mount annealing set-up layout. Heating was done by a hot plate with the pre-cut Mylar film between two flat ground glass to maintain the Mylar remain flat.

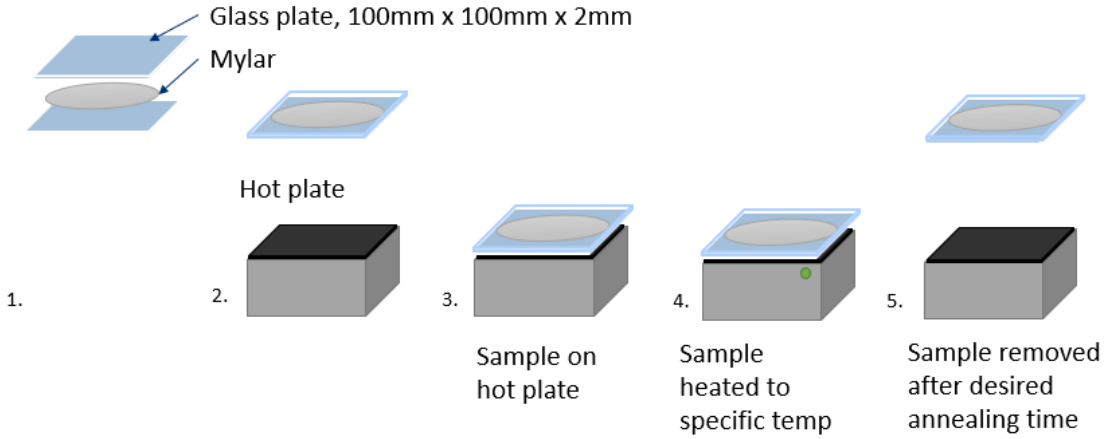

Figure 19. Pre-mount annealing set-up and process.

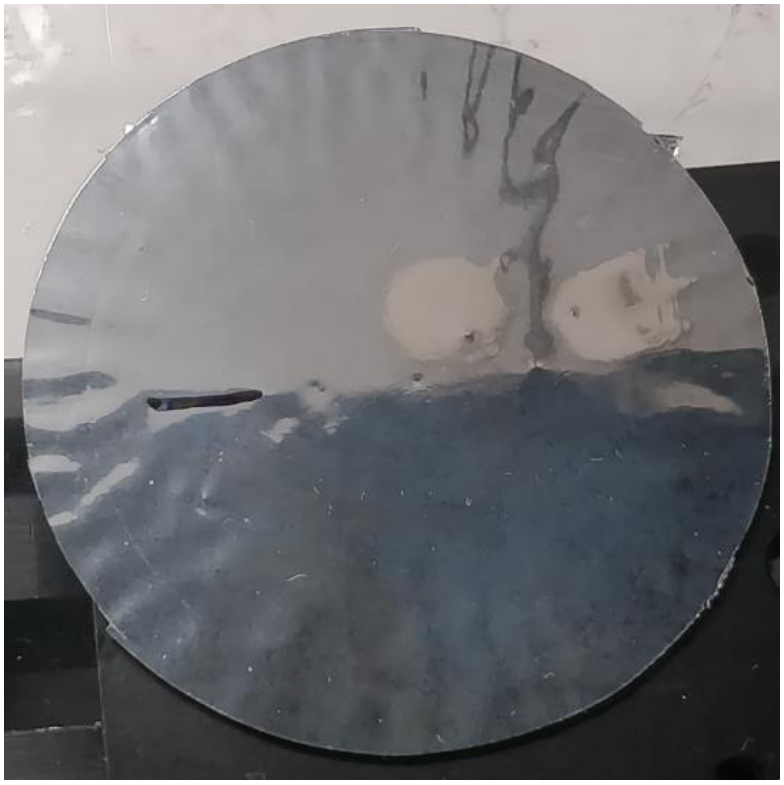

Figure 20. Image of wrinkles caused by pre-mount annealing at 140° C

3.8.1.3 Results

Figure 21-24 show the resulting image spot produced after the pre-mount annealing done on the Mylar. As mentioned before, when heating the Mylar at 140 ℃ there was significant wrinkling on the surface. Those wrinkles are exposed further by showing a spot image that appears to have significant scattering. At the lower temperature, there is less damage in the spot image but on close inspection, there is still some scattering seen compared to the untreated spot in Fig. 21. Table 2 list the size of the spot height and width of a non-anneal Mylar and anneal Mylar at 100, 120, and 140° C at the same negative pressure of 9%. As the lower temperature did show some reduction in spot size and the least amount of damage on the Mylar; it is plausible to say this method could be viable if tested with reduced temperature.

a) 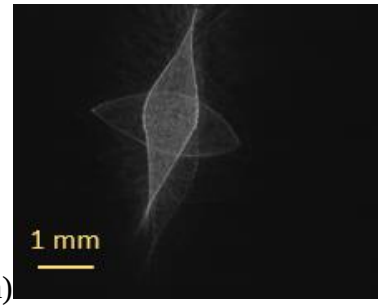

b) 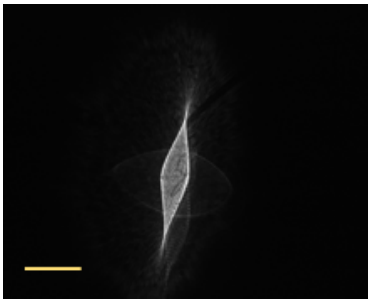
c) 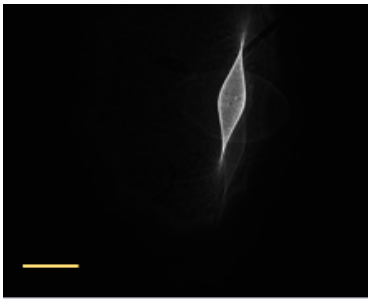

Figure 21. Images of a spot with no annealing prior to mounting and negative pressure applied.
a) medial focus at -2% (-0.3 psi) b) medial focus at -9% (-1.35 psi) c) medial focus at -15% (-2.25 psi).

Temp [C]\Time [hr]	1	2	3
100	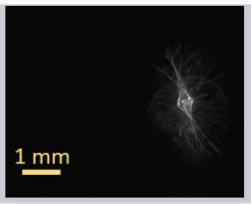	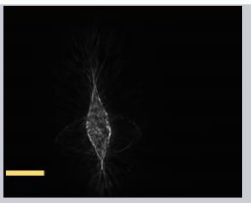	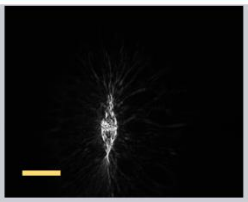
120	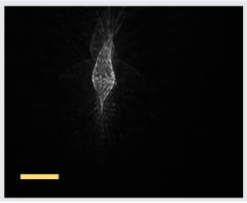	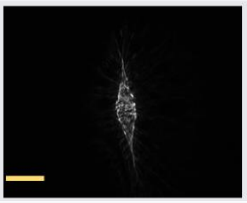	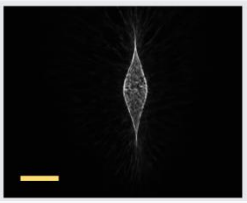
140	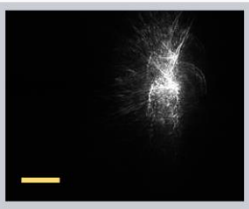	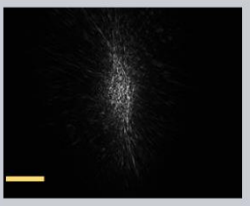	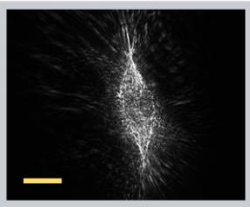

Figure 22. Spot images recorded at negative 2% pressure (0.3 psi)

Temp [C]\Time [hr]	1	2	3
100			
120	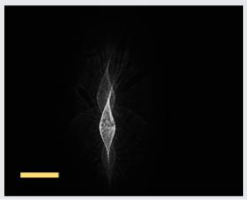	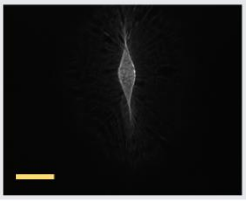	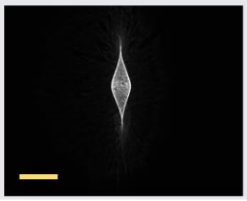
140	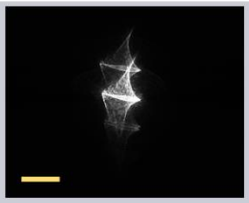	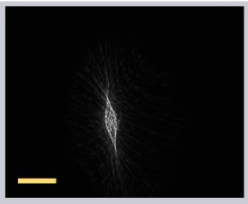	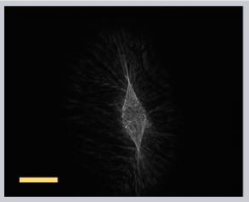

Figure 23. Spot images recorded at negative 9% pressure (1.35 psi)

Temp [C]\Time [hr]	1	2	3
100	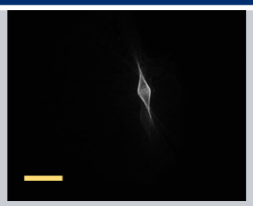	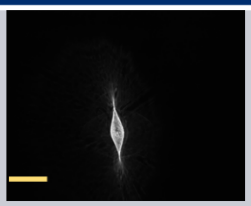	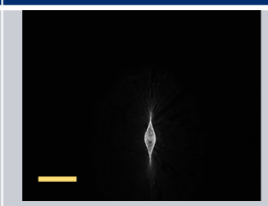
120	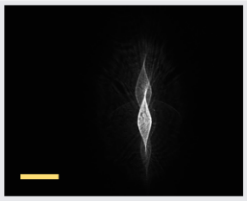	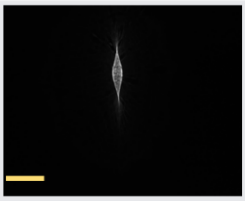	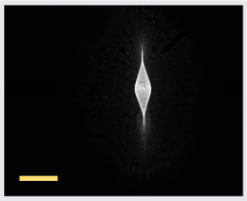
140	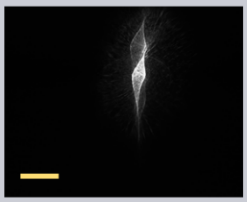	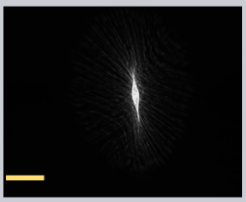	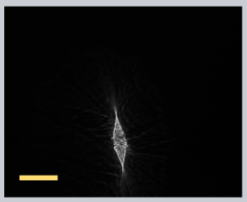

Figure 24. Spot images recorded at negative 15% pressure (2.25 psi)

Table 2 height and width of spot image for various temperature and time

Control	Width [mm]	Height [mm]								
2%	0.96	3.615								
9%	0.47	2.425								
15%	0.47	2.105								
@100C	Width [mm]	Height [mm]		@100C_2	Width [mm]	Height [mm]		@100C_3	Width [mm]	Height [mm]
2%	0.435	2.08		2%	0.665	2.55		2%	0.415	1.865
9%	0.445	1.945		9%	0.44	1.92		9%	0.28	1.43
15%	0.335	1.595		15%	0.355	1.6		15%	0.295	1.26
@120C	Width [mm]	Height [mm]		@120C_2	Width [mm]	Height [mm]		@120C_3	Width [mm]	Height [mm]
2%	0.665	2.14		2%	0.52	2.915		2%	0.645	2.695
9%	0.44	1.94		9%	0.45	2.05		9%	0.53	2.14
15%	0.38	1.875		15%	0.28	1.44		15%	0.44	1.925
@140C	Width [mm]	Height [mm]		@140C_2	Width [mm]	Height [mm]		@140C_3	Width [mm]	Height [mm]
2%	0.905	2.465		2%	0.67	2.365		2%	0.96	3.585
9%	0.505	2.135		9%	0.295	1.55		9%	0.615	2.155
15%	0.375	1.89		15%	0.2	1.27		15%	0.35	1.585

3.8.2 Mylar in-situ annealing

3.8.2.1 Set-up

The set up for the Mylar post-annealing composed of the original Mylar vacuum set up that is annealed with a modified heated coil. Since the Mylar mirror was oriented with the reflective surface facing upwards, the coils had to be mounted on a translation stage facing downwards.

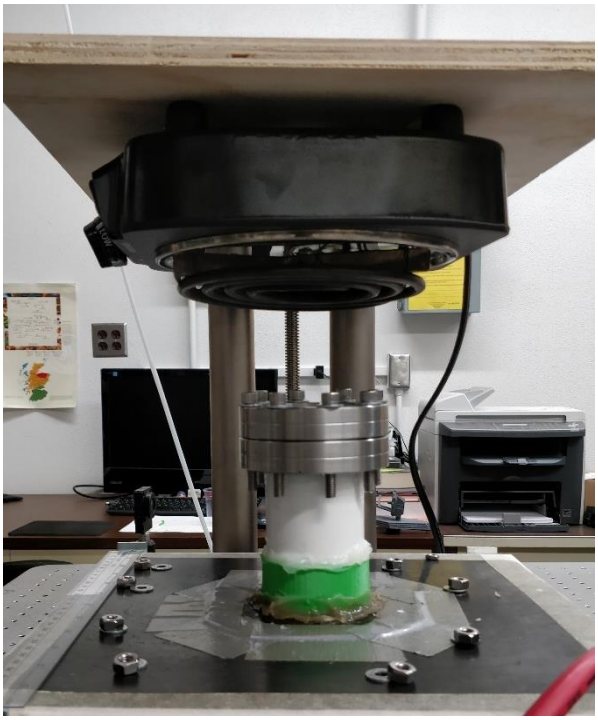

Figure 25. Image shows set-up for in situ annealing for Mylar mirror.

The internals of the coils was also altered. Originally when turned on, the coils would heat up and then turn off due to a thermostat in the connections. This would be a problem as it would not allow for consistent heating over a period. To solve this, the internals were opened and the wire that leads to the outlet plug was disconnected from the thermostat and connected directly to the coils. In doing this, when the wire is connected to the outlet it will then start running a current through the coils and begin to heat up. To be able to control the heat, the wire was connected to a variable transformer. With the variable transformer, the coils can now we turned on or off using the switch on the transformer. Also, the transformer has a dial that can specify the voltage that the coils get and allowing the Mylar mirror to be put under higher temperatures.

3.8.2.2 Testing procedures

The procedures in which the in-situ annealing was performed starts with applying an initial pressure. In the first testing situation, the Mylar mirror had 9% negative pressure applied, which is 1.35 psi. The mirror was set under the heating coils with a 4-inch separation. At 10 minutes per voltage, the Mylar is subjected to heat from 70,80, and 90V which corresponds to 52, 65, and 70 degree Celsius. Once 10 minutes have passed, the coils would be turned off and the radius of curvature of the mirror would be checked. Testing was also repeated with the coils mounted at a 3-inch separation rather than 4-inch with the same 9% negative pressure. Following that test, the separation remained at 3-inches but the pressure being applied during testing increased to 15% or 2.25 psi. After each test, the radius of curvature was measured to see the effect of the heating. Each test had a fresh sample of Mylar mounted to the mirror. Table 2 lays out the experimental conditions.

Table 3. Experiment conditions for in situ annealing

	Distance from heater	Voltage	Pressure
#1	4 inches	RT, 70, 80, 90	-9%
#2	3 inches	RT, 70, 80, 90	-9%
#3	3 inches	RT, 70, 80, 90	-15%

3.8.2.3 Results

Figure 26 plots the resulting radius of curvature for experiment 1 with heating at 48, 56, and 60-degree C. With these experiment conditions, a 4-inch distance between mirror and source, there is not a significant difference noticed. In experiment 2 in Fig 27, the source and mirror distance reduced to 3-inches. For this experiment, there is a noticeable difference between the Mylar mirror after the annealing and without annealing with an average change of 15 mm. Figure 28 shows the results for experiment 3, increasing the pressure during annealing. These results showed an increase in the radius of curvature change compared to experiment 2 having an average radii difference of 27 mm versus 15 mm.

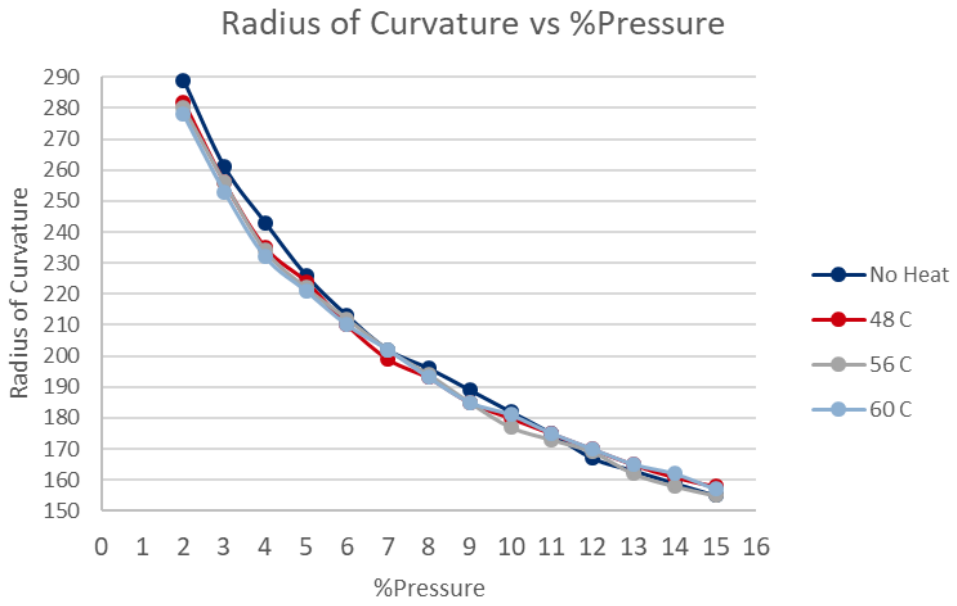

Figure 26. Experiment 1, heat source set at four inches away from Mylar. -9% pressure applied to Mylar. Voltages used for heat source yielded the shown temperature values. Time under heat is 10 minutes per temperature.

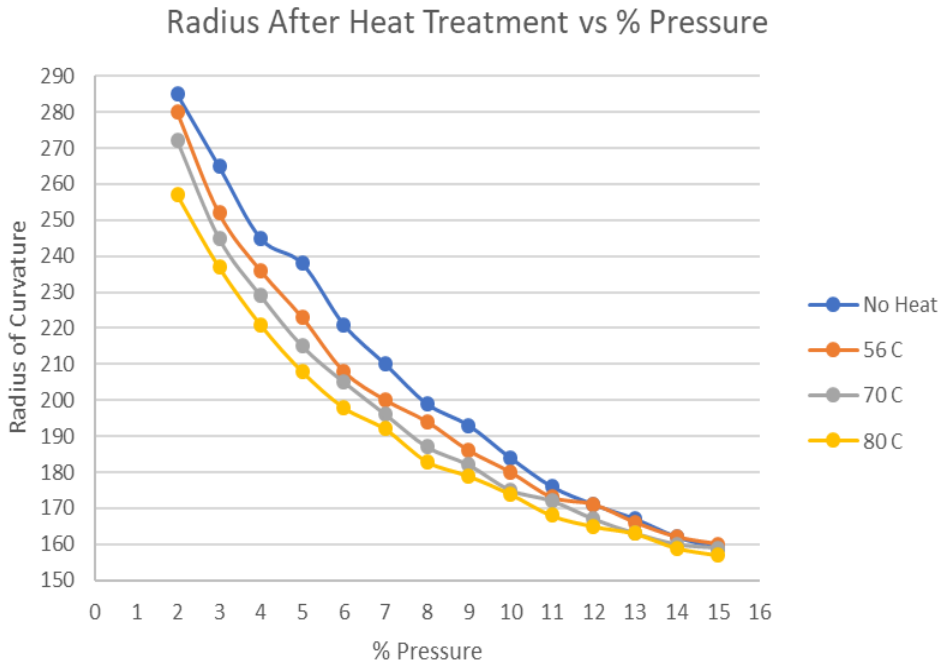

Figure 27. Experiment 2, heat source position changed to three inches away from the Mylar mirror. Same voltages were applied, but temperature values increased due to heat source distance. Time under heat remained 10 minutes.

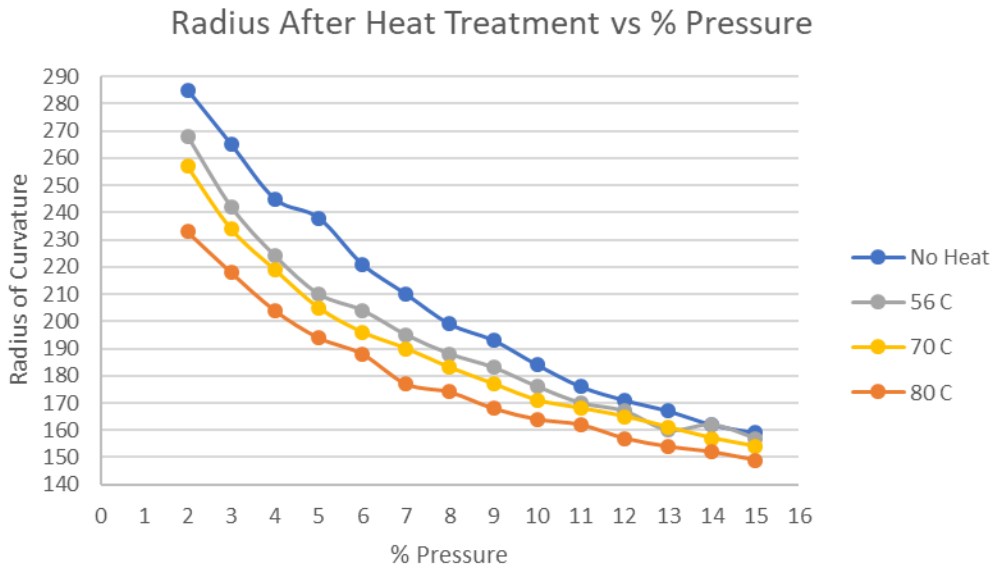

Figure 28 Experiment 3, the heat source position remained the same at three inches. Same voltages yielding the same temperatures. Time under heat remained at 10 minutes. Pressure applied to Mylar was increased from -9% to -15%.

Once the Mylar mirror was heat treated, the mirror was deflated and untouched for 24 hours. Coming back after 24 hours had passed, the mirror had the radius of curvature measured again. It

turns out that annealing the Mylar the heat from coils did not transfer enough to induce a stretch beyond the yielding point of Mylar. The Mylar had elasticity remaining and unstretched slightly from the amount measured from the previous day. However, the Mylar did not revert to the state it was before any heating was done. Overall, with the benefit of the in-situ annealing the reduce amount of pressure needed to achieve a specific radius of curvature is between 6-33% seen in the results plotted in Fig. 29 and displayed in Table 3. The large range is due to the larger difference in the lower pressure and the delta between the plot converging as it reaches the treatment curvature.

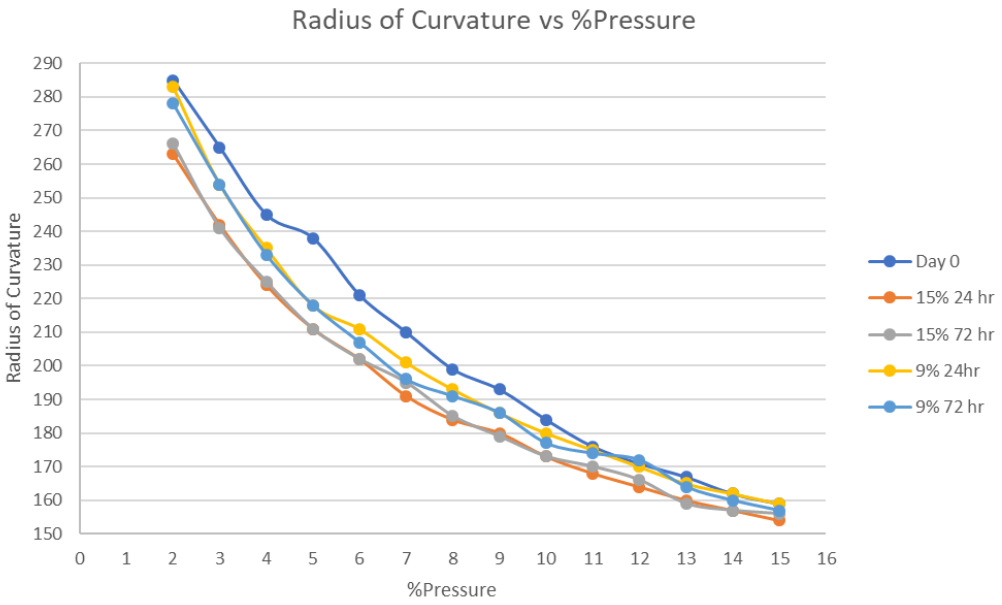

Figure 29. Post experiment 3. Induce radius of curvature change by heating decreases after a period of cooling

Table 4. The percent difference between pressure for a similar radius of curvature

%P (psi)	%P with equivalent R (psi)	P difference	% difference
2% (0.3)	3% (0.45)	0.15	33.3%
3% (0.45)	4.8% (0.72)	0.27	37.5%
4% (0.6)	5.8% (0.87)	0.27	31%
5% (0.75)	6.9% (1.035)	0.29	27.5%
6% (0.9)	7.6% (1.14)	0.24	21%
7% (1.05)	9.3% (1.395)	0.35	24.7%
8% (1.2)	10% (1.5)	0.3	20%
9% (1.35)	10.5% (1.575)	0.23	14.3%
10% (1.5)	12% (1.8)	0.3	16.7%
11% (1.65)	12.3% (1.845)	0.2	10.6%
12% (1.8)	12.8% (1.92)	0.12	6.25%
13% (1.95)	14.3% (2.145)	0.2	9.1%
14% (2.1)	15% (2.25)	0.15	6.7%
15% (2.25)	NA	NA	

3.8.3 Immersion annealing

An alternative mounting method for the Mylar led to a double-sided mounting design first inspired by a patent on air heating polyethylene balloon by Ehrreich, John E., Charles P. Fazio, and Beverly A. Nickerson [9]. In this architecture, two Mylar segments are attached to their own gasket. Etched into these gaskets was a groove to allow an air needle to be slotted in. The gaskets are then joined together and sealed using silicon. This set up would benefit from having a third middle gasket that is dedicated for the air inlet as it would not allow contact to the Mylar surface as it did for this quick proof of concept experiment.

Moving forward, the method of treating this Mylar mirror set up is having the set up submerged in heated water. The conditions for the experiment was water at 85° C and submerged for 30 seconds while pressure is being applied. The process of the immersion annealing is illustrated in

Fig. 30. Following the experiment, on first observation the magnification seen on the convex face of the mirror changed from before the mirror was submerged in the heated water, this can be seen in Fig. 31. With a change in magnification, it can be determined that the curvature of the Mylar had changed. This result gives another choice for mounting options with Mylar mirrors as well as a different method of heat treatment. This design if scaled up would resemble the model that L'Garde made for the IAE. In this testing, two rigid gaskets were used to hold the Mylar in place while it is believed that the IAE used an inflation ring to hold the membrane in place. If a rigid design were to be used for a larger scale mirror, a third ring should be incorporated for the inlet of air.

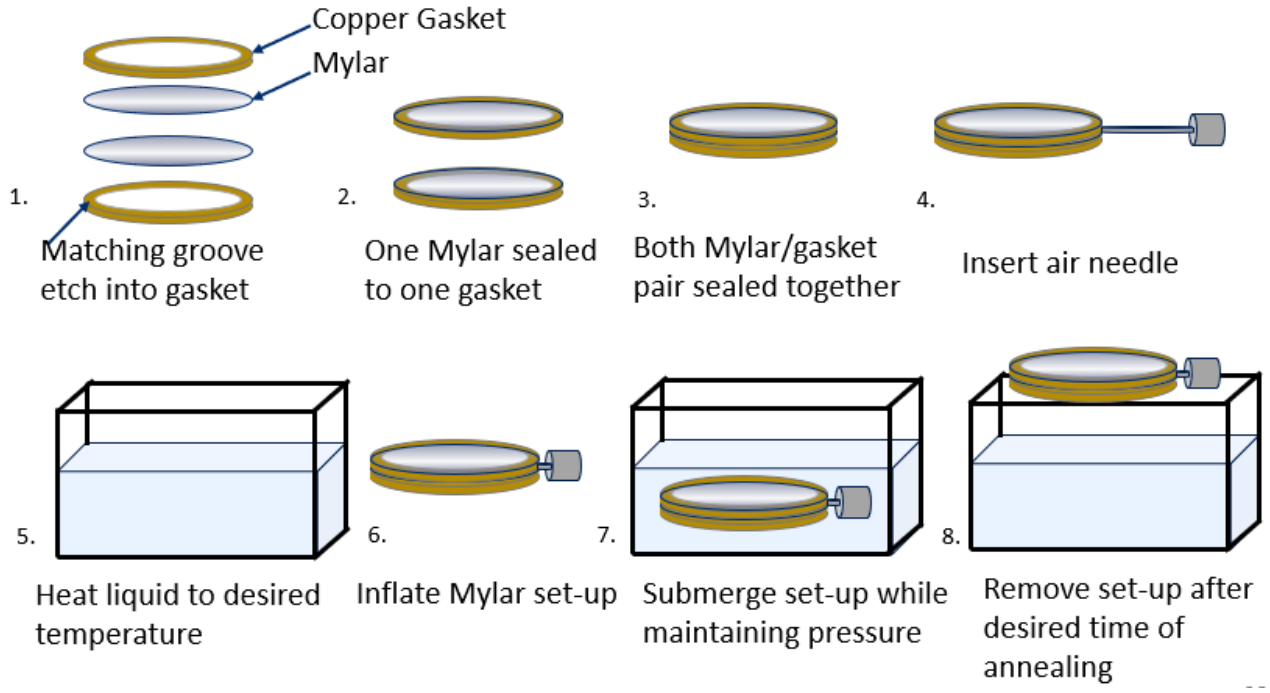

Figure 30. Fabrication and proess of immersion annealing

Figure 31. Left: Mylar Pre-Heat Treatment. Right: Mylar Post-Heat Treatment. Both images are taken of Mylar in air. A magnification change is noticed after Mylar had been subjected to heated water.

4 VACUUM MOLDED MIRROR

Exploring into alternative membrane mirror method, thicker PET was vacuum formed to create a solid mirror as compared to the Mylar mirror that changes the radii by pressure applied. These mirrors are created by taking a template then heating PET to be lowered on top using a vacuum to form the material to the curvature of the template. This process was done for this research by Rayama Pack co. For the sampled templates a biconvex lens with 300 mm radii (Rolyn Model # 11.0290), plano-convex with a 250 mm radius (Rolyn Model # 10.0453), and a concave mirror with a -2000 mm radius (Newport Model # 20DC2000ER.1) was provided to Rayama Pack. In the first batch of molded mirror samples, the thicknesses were 0.2 mm and 0.5 mm. Figure 32 is the visual inspection of the first batch. Immediately just from the images, there is a noticeable amount of error on the surface of these molded mirrors.

Mirror Specification	D = 50 mm, R = -300 mm	D = 50 mm, R = -2000 mm	D = 90 mm, R = -250 mm
T = 0.2 mm			
T = 0.5 mm		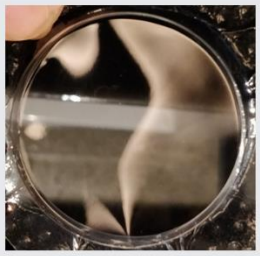	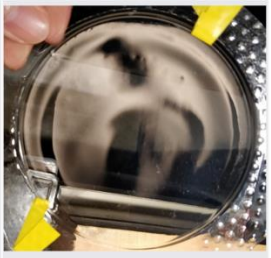

Figure 32. Visual inspection of molded mirror batch 1

Beam Dia.. on Mirror [mm]	D = 50 mm, R = -300, sample 1	D = 50 mm, R = -300, sample 2	D = 90 mm, R = -250
5	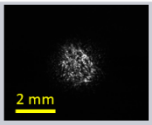 1.935 mm	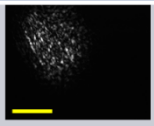 3.15 mm	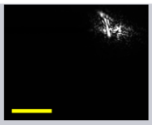 1.35 mm
10	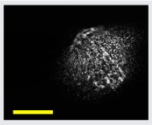 2.825 mm	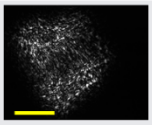 4.3 mm	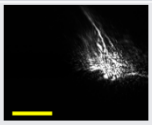 1.9 mm
15	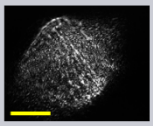 4.2 mm	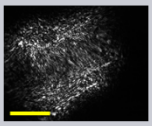 4.75 mm	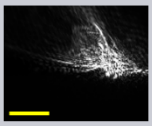 3.0 mm

Figure 33. Spot images from molded mirror batch 1 at various beam diameter

Using the same testing set up as was used on the Mylar mirror, the spot produced from these vacuum molded mirrors were recorded at varying beam diameter. Figure 33 shows the spots recorded from the molded mirror. Not all the samples from the first batch were recorded as some of the molded mirrors had a significant amount of errors on the surface that it would not produce a spot

on the camera. For the molded mirrors made from 0.5 mm thick PET, the surface quality visually appeared better than the 0.2 mm thick mirrors. Possible reasons for these flaws were the molded mirrors were stacked on top of each other and shipped in a regular bubble wrapped envelop. During transportation, the package was likely exposed to excessive heat of the carrying vehicles. For further evaluations of these types of mirrors, a request for thicker samples at 1 and 1.5 mm was asked. Better packaging considerations were highly encouraged as it would allow for untampered samples for testing.

Upon receiving the second batch, the packaging was much improved as can be immediately seen from the first visual inspections in Fig. 34-36. Overall, the thicker samples showed fewer distortions compared to the thinner samples of batch one. For this batch, the flaws in the surface were prominent around the outer edges of the mirror aperture. Figure 37 shows an example of the outer edge flaw. Along with the same issue, an edge line could be seen on the samples with 300 mm and 2000 mm radii. The possible cause for this could be the designed radius is too large for this manufacturing method or the material thickness isn't able to form around the template. It was also seen between two samples of the same thickness that the magnification was different among some of the designs.

Design R [mm]	Sample	T = 1 mm	T = 1.5 mm
250	#1	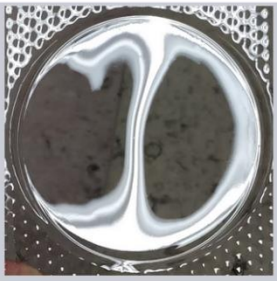	
250	#2	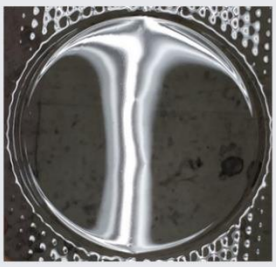	

Figure 34. Visual inspection of R = 250 mm for 1 and 1.5 mm thicknesses

Design R [mm]	Sample	T = 1 mm	T = 1.5 mm
300	#1		
300	#2		

Figure 35. visual inspection of R = 300 mm for 1 and 1.5 mm thicknesses

Design R [mm]	Sample	T = 1 mm	T = 1.5 mm
2000	#1		
2000	#2		

Figure 36. Visual inspection of R = 2000 mm for 1 and 1.5 mm thicknesses

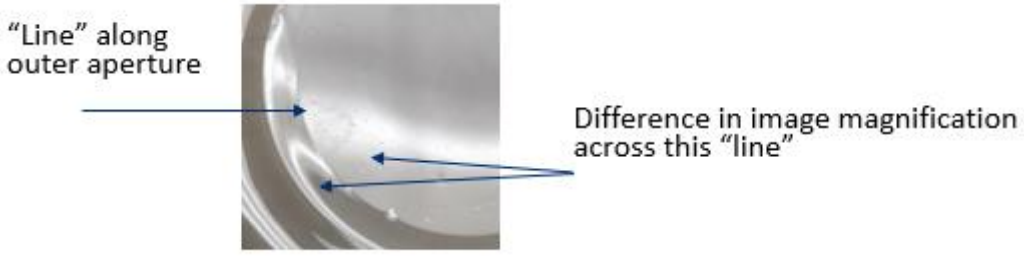

Figure 37. Image showing the line edge on the outer aperture of the molded mirror

Before imaging the spot on the camera, the radius of curvature was measured using the test set-up. Observed were some errors in forming the designed radius of curvature. For the first designed radius at 250 mm, for thickness 1 mm there was a difference of 100 mm between sample one and two. Sample one measured in at a radius of curvature of 180 mm and sample two with a value of 280 mm. Moving to the 1.5 mm thick samples of R=250 mm, the two samples produced the same value for their radius of curvature. Next with the 300 mm radius of curvature template at 1 mm thickness, sample one produced the correct curvature but unfortunately sample two couldn't produce

a focus. What was observed was the beam reflected off the mirror would diverge instead of converging. With the 1.5 mm thick samples for R=300 mm, both samples produced the same measured radius of curvature at 305 mm. Last with the design template of 2000 mm, neither sample at 1 mm thickness came into focus. The reflection from the mirrors was observed to be from a flat surface. For the 1.5 mm samples, these had the largest variance from their designed radius with both samples measured at 250 mm. For the 2000 mm template, it is possible the molded mirrors fail in their design in that the radius of curvature was too long to be molded at the material thickness. Table 4 list the results of the radius of curvature measurements.

Table 5. *1: mirror did not come into focus. Instead, the beam diverged after reflecting off the mirror. *2, *3: mirror did not come into focus. The observation was that the reflection was from a flat surface.

Design R [mm]	Sample	(T=1mm)	(T=1.5mm)
250	#1	180	280
	#2	280	280
300	#1	300	305
	#2	NA *1	305
2000	#1	NA *2	250
	#2	NA *3	250

Thickness [mm]	R = 250 mm	R = 300 mm	R = 2000 mm
0.2	NA*	NA*	NA*
0.5	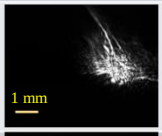 1.90mm Sample 1	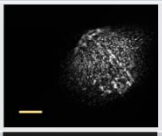 2.83mm Sample 1	NA*
1.0	 1.96mm Sample 2	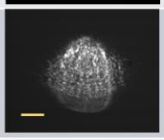 3.56mm Sample 1	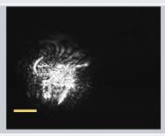 2.21mm Sample 2
1.5	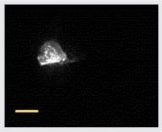 1.10mm Sample 2	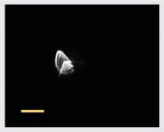 0.88mm Sample 2	 2.32mm Sample 2

Figure 38. Spot images of various thicknesses of the three radii molded mirror

Aside from the anomaly in the 2000 mm radius of curvature design, the images captured of the spots produced show that utilizing a thicker material for the mirrors can allow for a more condensed spot as laid out in Fig. 38. With the 300 mm mirrors yielding the best result and the least deviation from the designed radius of curvature, the request was made to have 2- and 3-mm thick samples.

Design R [mm]	Sample	T = 2 mm	T = 3 mm
300	#1	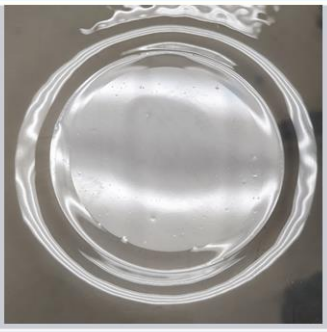	
300	#2		

Figure 39. Visual inspection of R = 300 mm for 2 and 3 mm thicknesses

For the 2- and 3-mm samples, a similar amount of distortion was seen based on the first visual inspections seen in Fig. 39. The previous line edge around the outer aperture was still present on these samples as well as shown in Fig. 37. A new surface default was noticed also seen on these samples in the form of “bubbles” on top of the material. These “bubbles” were not a product of the protective film that covered the back of the mirrors. Upon testing, these “bubbles” didn’t add any noticeable changes to the spot produced.

Table 5 shows the evaluation of the designed radius of curvature for these sample molded mirrors and this batch still yielded some offset measurement from what is expected. With the two samples at 2 mm thickness, one sample measured at the precisely designed radius while the second sample measured within 5% of the designed radius. Moving on to the 3 mm thick samples, there

were more noticeable defaults. One sample was measured within 10% of the designed radius and the other sample didn't produce a focus.

Figure 40-41 shows the observation of the spot produced by these molded mirrors. One 2 mm thick samples produced a spot with a diameter of 0.61 mm with a beam size of 20 mm. For the 3 mm thick sample, at the same beam size of 20 mm the spot produced had a measured diameter of 0.89 mm. An interesting observation from capturing images of these spots was at a beam of 10 mm the thicker sample produced at tighter focus at 0.28 mm vs 0.38 mm for the 2 mm sample.

Table 6. Focusing distance using the test set up of batch 3 molded mirrors.
*Mirror did not come into focus. The observation was that the reflection was from a flat surface.

Design R [mm]	Sample	(T=2mm)	(T=3mm)
300	#1	300	NA *
300	#2	290	330

Sample		w/Beam @ 10mm	w/Beam @ 15mm	w/Beam @20mm
1	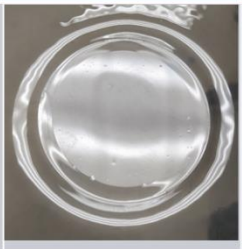	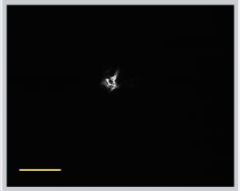 0.38 mm	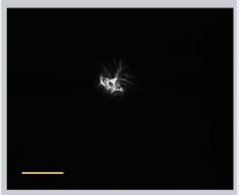 0.59 mm	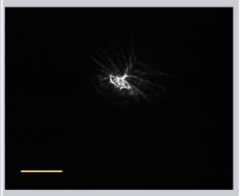 0.61 mm
2		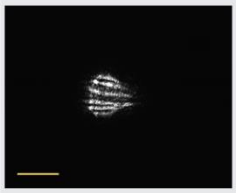 1.26 mm	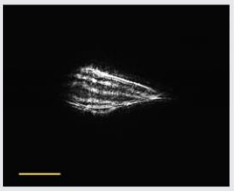 2.09 mm	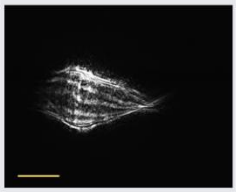 2.57 mm

Figure 40. Spot images from R = 300 mm, t = 2 mm molded mirror

Sample		w/Beam @ 10mm	w/Beam @ 15mm	w/Beam @20mm
1	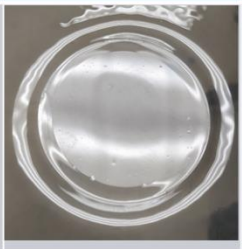	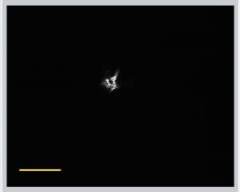 0.38 mm	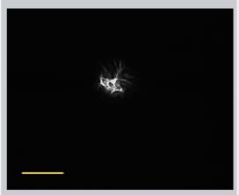 0.59 mm	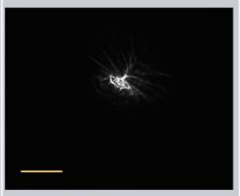 0.61 mm
2		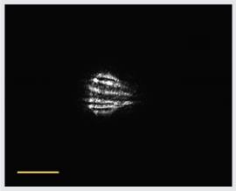 1.26 mm	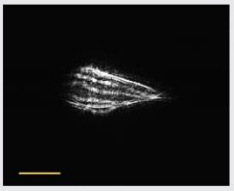 2.09 mm	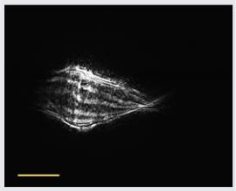 2.57 mm

Figure 41. Spot images from R = 300 mm, t = 3 mm molded mirror

Thickness [mm]	R design = 300 mm, Beam at 10 mm	R measured [mm]
0.5	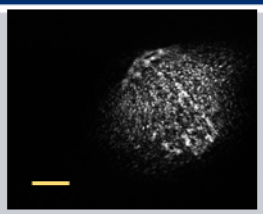 2.83mm Sample 1	303
1.0	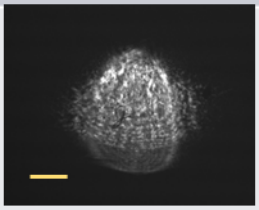 3.56mm Sample 1	300
1.5	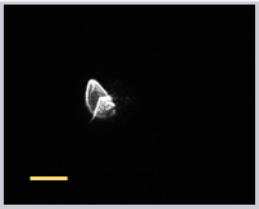 0.88mm Sample 2	305
2.0	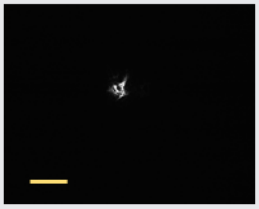 0.38 mm Sample 1	300
3.0	 0.28 mm Sample 2	330

Figure 42. Best spot images from each PET thickness

Figure 42 shows a comparison of the best spot produced by each thickness of the 300 mm designed molded mirrors. Sample 2 of the 3 mm thick material produced the tightest overall spot of the samples evaluated. With these results, it would be possible to conclude that using thicker material would yield tighter spots, but at 3 mm thickness, the produced radius of curvature was

offset by 10%. Moving backward to the 2 mm sample, there the measured radius of curvature didn't have a noticeable offset. While the spot from the 2 mm thick sample, at the same beam size, is larger than the spot of the 3 mm sample; at larger beam diameter the 2 mm thick sample produced smaller spots in comparison. Between the 2 mm and 3 mm samples, the spots produced are comparable to the spot produced by the Mylar mirror.

5 DISCUSSION

Through this research, it can be assessed that using a membrane mirror can be a viable option in place of conventionally made mirrors for use in THz range with some steps taken to maintain its fabrication. Simple insights and procedures have been made in the previous chapters on fabricating and annealing a small-scale system. From what was learned with the small-scale experimenting, the basic principles can be applied to a larger-scale system. A detail that was not brought up during the earlier chapters on fabricating the set-up is mounting the Mylar. Being a small-scale system, the weight of the copper gaskets kept the Mylar flat. When scaling up the system, this is likely not to work. To remedy this, it is suggested that the Mylar be laid on to a flat solid surface with some slight tension to smooth the film. The gasket or flange should then be set on top of the Mylar. From there the gasket or flange can have adhesive applied to it and the Mylar before the Mylar is cut to the circular shape.

As it was seen in lab results, there is pre-fabricated astigmatism manufactured into Mylar. Previous studies into Mylar have seen these results and have stated it is due to the material having a different yield in the orthogonal direction [5,7]. What was shown in this research was identifying the contributing aberrations by simulating the mirror in a lens design software. Sourcing an alternative material to remove the astigmatic shape was not as successful as the method in manufacturing Mylar or membrane films is to heat and stretch it to the desired thickness [10]. To be able to compensate for astigmatism as well as the spherical aberration would be to design compensating optics to accompany the Hencky surface of the intended aperture diameter. Earth telescope such as the Hobby Eberly Telescope has shown that a spherical based design can work as it has compensative optics to correct for the spherical aberration and other field aberrations. Though the Hencky surface isn’t a

spherical shape, the same approach can be taken to correct for the aberrations as Dr. Yuzuru Takashima has done for a future demonstration unit and possible space telescope. Using the findings of fabricating Mylar mirrors, it is possible to create a scaled-up version in shorter wavelengths. Aberrations caused by the shape formed can be corrected with the design of the telescope. An improvement for this research would have been adding adaptive optics to the testing set up to show the spot can be corrected. As for metrology, using deflectometry like the proposed method for Dr. Walker's TST concept would suffice as a Mylar telescope has the potential to be much larger than the traditional approach.

A second attempt was made to construct the directionality out of the Mylar, but it did not prevail. For larger scale mirrors, the use of the elliptical gaskets could reduce the astigmatic shape of a Mylar mirror. In the small-scale test, we reached the limit of what we were able to fabricate on our own but did show that the astigmatic medial focus could be controlled. Through heating the Mylar before mounting it was seen that it caused the surface of the mirror to be worse as can be seen with the spot images having more star flaring. When moving on to in situ heating, it was another method that did not induce any change to astigmatism seen in the spot image. What came from that experiment was how that curvature could be treated so it less pressure would be needed to provide a radius before the heat was applied. Heating through induction coils did show a slight reversal in the stretch produced resulting in about half the initial curative change to remain. The cause of this likely comes from the induction coils not transmitting efficiently as infrared heat mostly reflects off Mylar. A better method of transferring heat to Mylar to induce a stretch was having a mounted Mylar in contact with heated water as it showed a noticeable change in magnification for only being submerged in 85° C for 30 seconds.

With the vacuum molded mirrors, using thicker materials allowed for less distortion to be present due to handling. The problem that comes with thicker material would be limited aperture as it seemed there would hard edges towards the outer aperture. That aside, the spot size produced from the molded mirrors were on a similar order to that spot size seen from the Mylar mirror set up, although not as consistent as the Mylar mirror.

6 CONCLUSION AND FUTURE WORK

As surface roughness of Mylar is within' the λ/4 waves in peak-to-valley of surface roughness standard for the highest THz frequency, what is needed thereafter is having a controllable fabrication process of a Mylar mirror. From the experimentation that was done in this thesis, two designs have been discussed and procedures that will fit a build of necessary size; as well as what improvements that can be done that came from the experiments.

Two forms of annealing have been presented: a pre-mount annealing and in-situ annealing. From these experiments, the pre-mount annealing allowed for higher heat transfer, but at the possible cost of damaging the Mylar. With in-situ annealing, this method allows for gradual heating as it is an infrared source and most of the heat is reflected by the Mylar. The method of annealing the double-sided Mylar design is a combination of both previous methods by having the Mylar mounted while having better heat transfer with the heated water.

Everything from this research considered, the work has been done on a single continuous sheet of Mylar. So, when considering scaling up, it is more likely that the Mylar won't be a singular sheet without having to make a large version of the machinery needed to make Mylar. Since multiple sheets or rolls of Mylar would likely be used to create a larger system, a look the best possible method of attaching sheets together is best to be observed. When attaching sheets of Mylar to create one larger surface, it would be best to keep the direction of the Mylar the same. Doing this would allow the work in this research to be maintained and usable. Most notably with astigmatism that comes from a Mylar mirror when attaching sheets together as crisscrossing sheets could create a freeform surface that is more difficult to correct. Another possibility to the crisscross of Mylar sheets

is having a behavior like the double layer Mylar from section 3.9 where the astigmatic spot was larger.

Moving forward in future work, it has already been seen that with the Mylar mirror it is not rotationally symmetric, but it would be beneficial to take a scan of the surface of a Mylar mirror to directly compare it to the model of a Hencky curve. With a better understanding and comparison to a Hencky curve that a Mylar mirror produces, especially one which incorporates attached Mylar sheets. Efforts in performing a scan of the surface are planned for a 1-meter scale Mylar mirror. With the 1-meter scale Mylar mirror it will be based off the double side mounting set up that was explored in Section 3.10. Improvements that were concluded from that experiments have been incorporated into a better design, such as using three flanges so the air inlet has a dedicated entry and Mylar sheets will be separated by the middle flange. Figure 43 shows the CAD modeling of the planned build of this Mylar mirror. The 1-meter design will also employ the annealing by heated water instead of the coils as tests showed better heat transfer. This 1-meter scale Mylar mirror will be fabricated as a small-scale demo unit intended for a proposal by Dr. Chris Walker to design and fabricate a 20-meter Mylar space telescope mission.

For this mission, Dr. Walker is planning to collaborate with L'Garde in the build of this Mylar telescope as they have prior experience in building a similar design and having it fail in certain areas. Originally, Dr. Walker proposed a 14-meter design, but after a trade study was done by Dr. Takashima, a 20-meter design was decided upon. This 20-meter design will have an effective aperture of 14-meters and the increase to the primary would allow a size reduction of the corrective optics for better transport into space. Table 7 shows the trade study done by Dr. Takashima. Figure 44 plots the reduction in diameter of M2 and M3 with the estimated weight with a 14-meter Mylar

primary and a 20-meter Mylar primary. So by increasing the size of the Mylar primary mirror from 14-meter to 20-meter, the estimated weight of the corrective optics drops from 596 kg to 170 kg. The reduction in weight of the corrective optics come at the cost of a larger primary and extended supports, but with communications to L'Garde, they are confident it won't be an issue to construct or reduced strength with longer supports. The estimated sag of the 20-meter Mylar primary mirror would need a pressure of 0.063 psi of Helium to produce the necessary shape. At that pressure and volume of the enclosure, the approximate weight of He needed is 0.615 kg. Utilizing the research done in this thesis with annealing, it is estimated the pressure can be reduced by 30% to produce the same curvature needed for the 20-meter primary. The reduction reduces the pressure needed to 0.044 psi of He, which approximates to 0.430 kg. That same weight reduction transfers over to the weight of He needed to maintain the mirror over a 2 year mission with an approximate 5% leak rate per day the 20-meter Mylar primary would need 42.6 kg of He. For an 20-meter Mylar primary with annealing, the amount of gas needed for a two year mission would reduce to 29.8 kg. Table 8 list the total weight saving of the 14-meter, 20-meter, and 20-meter with annealing. In that table it can be seen that the 14-meter mirror has more weight of He gas than the 20-meter design. This is due to the simulated design of the 14-meter mirror having a larger sag compared to the 20-meter design and therefore requiring more pressure to achieve the desired shape. With the findings in this thesis, work has already started on a 1-meter Mylar mirror and annealing techniques that could remedy the issue that L'Garde experienced during their mission by reducing the amount of gas needed to obtain the desired curvature for their instruments would allow for a higher chance of a successful mission.

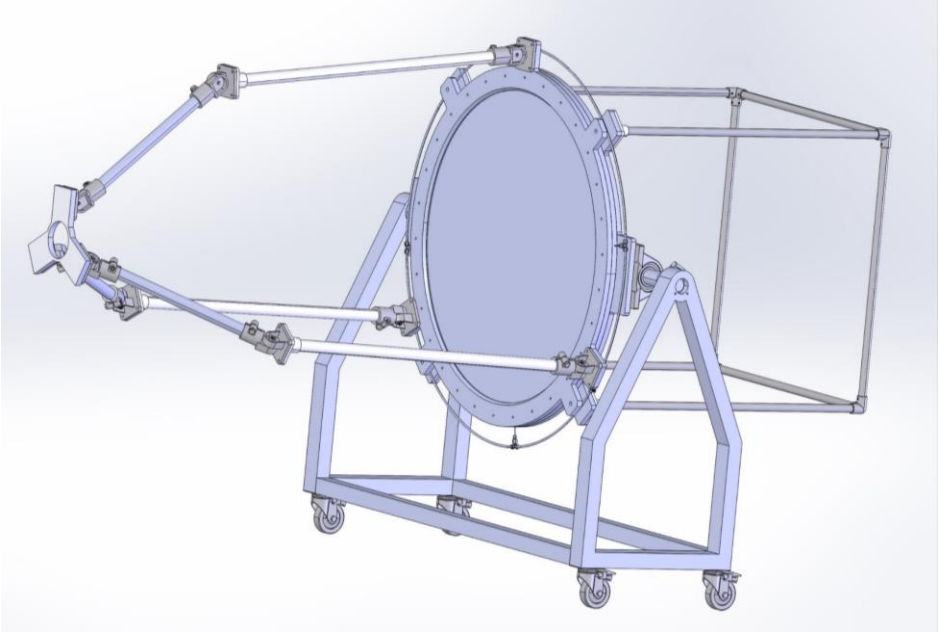

Figure 43. CAD model of 1-meter Mylar mirror demo unit.

Table 7. Trade study done by Dr. Takashima on diameter reduction of M2 and M3 with increased diameter of Mylar primary.

D: Diameter of Ring	File	M2 dimeter [m]	M3 diameter [m]	L: M1 to M2 distance	Rout [m]	Rin [m]	Area [m^2]
14	D14	3.048	1.824	24.38	7	3.26	120.5504
15	D15	2.728	1.694	26.484	7	3.7	110.9296
16	D16	2.516	1.56	28.684	7	3.73	110.2294
18	D18	2.252	1.384	33.184	7	3.7	110.9296
20	D20	1.964	1.242	37.38	7	3.7	110.9296
22	D22	1.692	1.13	41	7	4.2	98.52035

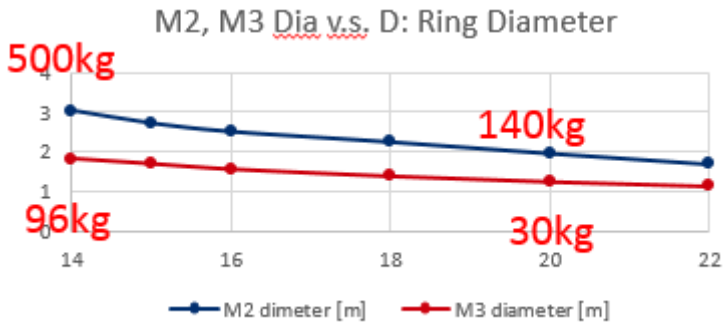

Figure 44. Plot of M2 and M3 diameter reduction with the increase of Mylar primary diameter increase. Weight of M2 and M3 estimatation labeled at 14m Mylar primary and 20m Mylar primary.

Table 8. Estimation of weight saving benefit of 20m Mylar mirror with and without annealing.

Design	Mylar Weight [Kg]	2 year mission Gas Weight [Kg]	Corrector [Kg]	Total Weight [Kg]
OASIS 14m	10.6	150	596	756.6
OASIS 20m	21.7	42.6	170	234.3
OASIS 20m with annealing	21.7	29.8	170	221.5

APPENDIX

Deflectometry

For evaluation of the primary mirror, deflectometry is used to perform the measurements. Deflectometry is done by performing a measurement of the 2-dimensional slope map of the optic under test. The setup is composed of a screen that is reflected off the test optic and is recorded by a camera. Screen geometry of the screen being used is known, as is the test optics and camera position, the local slopes of the surface being tested can be calculated. Using the derived slopes, a map of the surface sag can be obtained. Specifically, for this mirror, the method used is phase shifting deflectometry. This method has the screen source display a sinusoidal pattern that is shifted. The image produced is used to unwrap the phase and obtain the source coordinates [11,12,13].

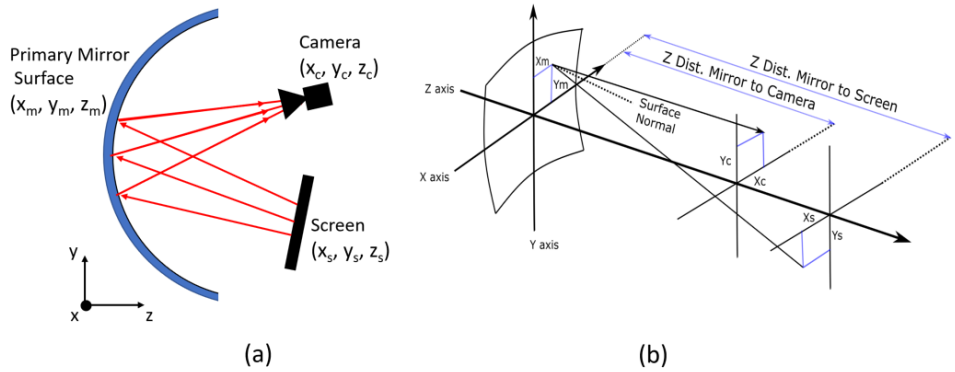

Figure 45. The screen acts as a source in a deflectometry system, whose light is reflected from the primary mirror surface and captured by a camera (a). By knowing the coordinates of the camera, mirror, and screen the local surface normal can be calculated for points on the primary mirror surface (b).

REFERENCES

[1] Walker, Christopher K., et al. "Spherical reflectors for space based telescopes." 2017 IEEE MTT-S International Microwave Symposium (IMS). IEEE, 2017.

[2] Walker, Chris. “Re: Question on balloon”. Received by Andy Phan, 11 April 2019.

[3] Films, DuPont Teijin. "Mylar® polyester film, Product Information." 222367D, Jun (2003).

[4] Freeland, R. E., et al. "Large inflatable deployable antenna flight experiment results." Acta Astronautica 41.4-10 (1997): 267-277.

[5] Meinel, Aden B., and Marjorie P. Meinel. "Inflatable membrane mirrors for optical passband imagery." Optical Engineering39.2 (2000): 541-551.

[6] “Hobby-Eberly Telescope.” *Hobby-Eberly Telescope | McDonald Observatory*, The University of Texas McDonald Observatory, mcdonaldobservatory.org/research/telescopes/HET.

[7] Savage, Richard, et al. "Current Status of the Hobby-Eberly Telescope wide field upgrade." Ground-based and Airborne Telescopes III. Vol. 7733. International Society for Optics and Photonics, 2010.

[8] Holenstein, Bruce D., et al. "Experiments with pneumatically-formed metalized polyester mirrors." Lightweight alt-az telescope developments, eds. Genet R, Johnson J, Wallen V (Collins Foundation Press, Santa Margarita, 2010a) (2010): 381-394.

[9] Ehrreich, John E., Charles P. Fazio, and Beverly A. Nickerson. "Polyethylene balloon." U.S. Patent No. 3,149,017. 15 Sep. 1964.

[10] Helmenstine, Anne Marie, Ph.D. "What Is Mylar?" ThoughtCo, Sep. 17, 2018, thoughtco.com/mylar-polyester-film-608929.

[11] E. Lowman, G. A. Smith, L. Harrison, S. C. West, and C. J. Oh, "Measurement of large on-axis and off-axis mirrors using software configurable optical test system (SCOTS)," in *Advances in Optical and Mechanical Technologies for Telescopes and Instrumentation III* (International Society for Optics and Photonics, 2018), Vol. 10706, p. 107061E.

[12] R. Huang, P. Su, T. Horne, G. B. Zappellini, and J. H. Burge, "Measurement of a large deformable aspherical mirror using SCOTS (Software Configurable Optical Test System)," in *Optical Manufacturing and Testing X* (International Society for Optics and Photonics, 2013), Vol. 8838, p. 883807.

[13] R. Huang, "High precision optical surface metrology using deflectometry," Ph.D., The University of Arizona (2015).